

Fermi-Luttinger liquid: spectral function of interacting one-dimensional fermions

M. Khodas,¹ M. Pustilnik,² A. Kamenev,³ and L.I. Glazman¹

¹*William I. Fine Theoretical Physics Institute and School of Physics and Astronomy,
University of Minnesota, Minneapolis, MN 55455*

²*School of Physics, Georgia Institute of Technology, Atlanta, GA 30332*

³*School of Physics and Astronomy, University of Minnesota, Minneapolis, MN 55455*

We evaluate the spectral function of interacting fermions in one dimension. Contrary to the Tomonaga-Luttinger model, our treatment accounts for the nonlinearity of the free fermion spectrum. In a striking departure from the Luttinger liquid theory, the spectrum nonlinearity restores the main feature of the Fermi liquid: a Lorentzian peak in the spectral function on the *particle* mass-shell. At the same time, the spectral function displays a power-law singularity on the *hole* mass-shell, similar to that in the Luttinger liquid.

PACS numbers: 05.30.Fk, 71.10.-w, 71.10.Pm

I. INTRODUCTION

One-dimensional problems play a special role in quantum many-body theory. In many cases, the reduced dimensionality affords one a deeper understanding of the role of interactions in a many-body system. Recent progress in experimental techniques has also contributed to the increased attention paid to a variety of one-dimensional (1D) fermionic and bosonic systems. Examples include edge modes of the quantum Hall liquid¹, carbon nanotubes², cleaved edge semiconductor wires³, antiferromagnetic spin chains⁴, and cold atoms in 1D optical traps⁵. These developments catalyze the interest to the fundamental theory of interacting 1D quantum liquids⁶⁻¹².

The traditional framework for discussing 1D systems is provided by the exactly solvable Tomonaga-Luttinger (TL) model¹³⁻¹⁵. The crucial simplification that makes the model solvable is the linearization of the fermionic dispersion relation. It was understood early on¹⁴ that a model with a linear spectrum is an idealized one. The goal of this paper is to elucidate the influence of the dispersion nonlinearity on the spectral function of 1D Fermi systems.

In the absence of interactions, the spectral function is given by $A_p(\epsilon) = \delta(\epsilon - \xi_p)$, where ξ_p is the single-particle energy measured relative to the Fermi level ($\xi_p = p^2/2m - \epsilon_F$ for Galilean-invariant systems). According to the Fermi liquid theory¹⁶, weak repulsive interactions merely broaden the peak in $A_p(\epsilon)$ to a Lorentzian,

$$A_p(\epsilon) \propto -\text{Im} \frac{1}{\epsilon - \xi_p + i/2\tau_p}, \quad (1)$$

The broadening originates in the finite decay rate $1/2\tau_p$ of the Fermi liquid quasiparticles. The rate can be estimated with the help of the Golden Rule,

$$\frac{1}{2\tau_p} \sim (D-1)(\nu V)^2 \frac{\xi_p^2}{\epsilon_F}, \quad (2)$$

where ν is D -dimensional density of states and V is the characteristic strength of the short-range repulsive

interaction. Indeed, quasiparticle relaxation occurs via real transitions resulting in the excitation of particle-hole pairs. In dimensions $D > 1$ already a single pair produces a finite decay rate. The amplitude of such process is proportional to V , hence the dimensionless factor $(\nu V)^2$ in Eq. (2). The factor ξ_p^2 accounts for the corresponding phase space volume, i.e. the number of possibilities a pair can be excited while obeying the energy and momentum conservation laws.

In 1D the situation differs dramatically. Indeed, the Golden Rule result Eq. (2) is identically zero for $D = 1$. Moreover, it can be shown¹⁷ that in the framework of the TL model¹³⁻¹⁵, the self-energy vanishes on the mass-shell in *all* orders of the perturbation theory. In fact, the TL Green function^{17,18} assumes manifestly non-Fermi liquid form. In the vicinity of the mass-shell, $|\epsilon - \xi_k| \ll |\xi_k|$, it reads

$$G_k(\epsilon) \propto \left(\frac{-\text{sgn} \xi_k}{\epsilon - \xi_k + i0} \right)^{1-\gamma_0^2}, \quad (3)$$

where $k = p - p_F$ and $\xi_k = \pm vk$ is the dispersion relation linearized near the right (left) Fermi point $\pm p_F$. The corresponding spectral function of, say, the right-moving excitations then takes the form (hereinafter we concentrate on the limit of zero temperature¹⁹)

$$A_k(\epsilon) \sim \frac{\gamma_0^2}{|\epsilon - \xi_k|^{1-\gamma_0^2}} \theta[(\epsilon - \xi_k) \text{sgn} \xi_k]. \quad (4)$$

The exponent γ_0 in Eqs. (3) and (4) characterizes the interaction strength and in the lowest order is given by

$$\gamma_0 = \frac{1}{2} \nu (V_0 - V_{2p_F}), \quad (5)$$

where $\nu = (2\pi v)^{-1}$ is the density of states in 1D and V_k is the Fourier transform of a short-range interaction potential.

Unlike the Fermi-liquid Lorentzian Eq. (1), the spectral function Eq. (4) exhibits a characteristic threshold behavior. The edges of the spectral support coincide with the single-particle energies ξ_k , and the spectral function

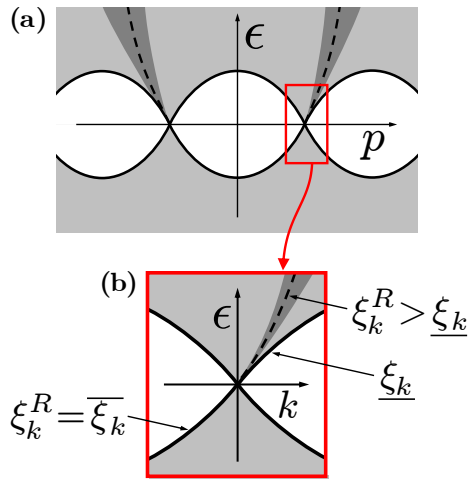


FIG. 1: (a) Support of the spectral function in (p, ϵ) -plane. The parabola represents the mass-shell ($\epsilon = \xi_p$). For $\epsilon < 0$, the mass-shell coincides with the edge of the spectral support. For $\epsilon > 0$, however, the mass-shell (dashed lines) falls into a broad spectral continuum. In this region, the spectral function has a peak of a finite width, which is indicated schematically by dark gray. (b) The low-energy region near the right Fermi point $p = p_F$, with $k = p - p_F$.

displays a power-law edge singularity on the mass-shell $\epsilon \rightarrow \xi_k$. This singularity is a hallmark of the Luttinger liquid²⁰ behavior. The particle-hole symmetry of the TL

model implies that $A_k(\epsilon) = A_{-k}(-\epsilon)$, hence the behavior of $A_k(\epsilon)$ in the particle region of the spectrum $\epsilon > 0$ is identical to that in the hole region $\epsilon < 0$.

The exact solvability of the TL model relies crucially on the assumption of strictly linear dispersion relation. The purpose of this paper is to examine the effects of the dispersion nonlinearity on the spectral function of 1D spinless fermions. Specifically, we consider a non-linear dispersion relation with a positive curvature, and approximate the single-particle spectrum in the vicinity of the right (R) and left (L) Fermi points by

$$\xi_k^{R/L} = \pm vk + \frac{k^2}{2m} + \dots, \quad k = p \mp p_F. \quad (6)$$

The presence of a finite mass m breaks the particle-hole symmetry of the TL model and affects the spectral function in the particle and hole regions of the spectrum in manifestly different ways.

The effect of the dispersion nonlinearity on the *particle* region $\epsilon > 0$ is the most dramatic. Rather than being the edge of the spectral support, the mass-shell $\epsilon = \xi_k^R$ now falls within a broader continuum, see Fig. 1. Consequently, the edge singularity [cf. Eq. (4)] on the mass-shell disappears and gets replaced by a peak of a finite height. Both the shape and the width of the peak appear to be rather different from those in $D > 1$, see Eqs. (1) and (2). For $\epsilon > 0$ and $|\epsilon - \xi_k^R| \lesssim k^2/2m$ we found

$$A_k(\epsilon) \propto \text{Im} \left\{ \frac{\mu_{2p_F+k}^2}{\gamma_k^2} \left(\frac{-1}{\epsilon - \xi_k^R + i/2\tau_k} \right)^{1-\gamma_k^2} - \frac{\mu_k^2}{\gamma_k^2} \left(\frac{1}{\epsilon - \xi_k^R + i/2\tau_k} \right)^{1-\gamma_k^2} \right\}. \quad (7)$$

The k -dependent exponent γ_k is given by

$$\gamma_k^2 = \frac{1}{4}(\mu_{2p_F+k}^2 + \mu_k^2), \quad (8)$$

where

$$\mu_k = \nu(V_0 - V_k) \frac{2mv}{|k|} \quad (9)$$

is the exponent governing the power-law divergence of the dynamic structure factor⁸. For short-range interactions $\mu_k \rightarrow 0$ when $k \rightarrow 0$, while $\mu_{2p_F} = 2\gamma_0$, hence $k \rightarrow 0$ limit of Eq. (8) agrees with Eq. (5).

The main feature of Eq. (7) is the appearance of a finite quasiparticle decay rate, $1/2\tau_k$. To the lowest non-vanishing order in the interaction strength it is given by

$$\frac{1}{2\tau_k} = C[\nu^2 V_0(V_0 - V_k)]^2 \frac{(\xi_k^R)^4}{(mv^2)^3}, \quad C = \frac{3^3 \pi}{5 \cdot 2^9} \approx 0.03. \quad (10)$$

A finite decay rate emerges only in the fourth order in the interaction strength²¹. This is because the minimal relaxation process involves excitation of two particle-hole pairs on the opposite branches of the spectrum. The factor $(\xi_k^R)^4$ in Eq. (10) accounts for the corresponding phase space volume. Note also that $1/\tau_k \propto m^{-3}$ and vanishes in the limit $m \rightarrow \infty$ taken at a fixed v , which corresponds to the TL model.

Despite its small value compared to that in higher dimensions, the very emergence of a finite quasiparticle relaxation rate in a 1D system is a matter of fundamental significance. One may even wonder if it puts 1D Fermi systems back in the realm of the conventional Fermi liquid theory. Indeed, in a broad region $|\epsilon - \xi_k^R| \lesssim (\tau_k \gamma_k^2)^{-1}$ around the mass-shell, the spectral function Eq. (7) is essentially a Lorentzian with the width $1/\tau_k \ll (\tau_k \gamma_k^2)^{-1} \ll \xi_k^R$, see Fig. 2. Restoring all the factors, we find for the immediate vicinity of the particle

mass-shell, $|\epsilon - \xi_k^R| \lesssim (\tau_k \gamma_k^2)^{-1}$,

$$A_k(\epsilon) = \frac{1}{\pi} \left(\frac{k}{mv} \right)^{3\gamma_0^2} \left(\frac{m}{k^2 \tau_k} \right)^{\gamma_k^2} \frac{1/2\tau_k}{(\epsilon - \xi_k^R)^2 + 1/4\tau_k^2}. \quad (11)$$

Furthermore, for not too small momenta, such that

$$\ln(k/p_F) \gtrsim -\frac{1}{\gamma_0^2} \quad (12)$$

(this condition allows for $k \ll p_F$ at $\gamma_0 \ll 1$) the Lorentzian peak (11) carries most of the particle's spectral weight, see Section VII. This is the hallmark of the Fermi liquid¹⁶. The Luttinger liquid behavior is found only at smaller momenta and sufficiently far away from the mass-shell, at $|\epsilon - \xi_k^R| \gg (\tau_k \gamma_k^2)^{-1}$.

The dispersion nonlinearity has a strong effect on the spectral function despite being irrelevant in the renormalization group (RG) sense: it does not affect, for example, the power-law asymptote of the local tunneling density of states at low energies. However, momentum-resolved measurements^{3,4} and numerical simulations⁹ may reveal the structure of the quasiparticle peak near the particle mass-shell.

In the hole region of the spectrum $\epsilon < 0$, the positive dispersion curvature does not smear the TL power-law singularity at the mass-shell. The singularity is preserved because due to kinematic constraints, the hole mass-shell remains to be the edge of the spectral support (see the next section). The only effect of the spectrum nonlinearity is the renormalization of the exponent in the hole part of the spectral function [cf. Eq. (4)],

$$A_k(\epsilon) \propto \frac{\gamma_k^2}{(\xi_k^R - \epsilon)^{1-\gamma_k^2}} \theta(\xi_k^R - \epsilon), \quad (13)$$

where $\xi_k^R - \epsilon \ll k^2/2m$ and the exponent γ_k^2 is given by Eq. (8). Note that the exponent is invariant upon momentum inversion $k \leftrightarrow 2p_F + k$ and interpolates smoothly between the two Fermi points; Eq. (13) is applicable

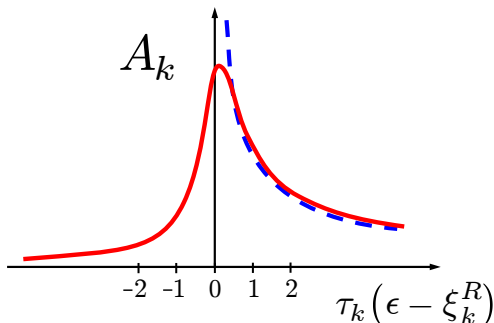


FIG. 2: Spectral function in the vicinity of the particle mass-shell $\epsilon \approx \xi_k^R > 0$. The solid line is a plot of Eq. (7) with $\mu_{2p_F+k} = 1.1$, $\mu_k = 0.4$, and γ_k given by Eq. (8). For comparison, the dashed line corresponding to the Luttinger liquid result Eq. (4) is also shown.

along the entire hole mass-shell line, see Fig. 1. The quadratic dependence of the exponent on the interaction strength originates in the orthogonality catastrophe phenomenon²². Further away from the hole mass-shell the spectral function crosses over to the TL one, Eq. (4).

We described above the behavior of the spectral function close to the mass-shell. The regions of a finite spectral weight are indicated by the shaded area in Fig. 1. Apart from the hole mass-shell, all edges of the spectral support are characterized by the power-law behavior of the spectral function with momentum-dependent *positive* exponents. This is easy to foresee, if one notices that the states responsible for the nonzero spectral weight far from the single-particle mass-shell must involve several excitations. The main contributions to the values of the exponents come from the constraints on the phase space available for such excitations. The additional contribution to the exponents is due to the interaction between the excited particles and holes. This contribution is first-order in the interaction potential and has the same origin as the the exponents in the X-ray singularity phenomenon²³. A detailed theory of the threshold behavior of the spectral function is developed in Section V.

The rest of the paper is organized as follows: In Section II we present a qualitative analysis of the problem. Perturbative calculation of $1/\tau_k$ to fourth order in the interaction strength is carried out in detail in Section III. In Section IV we develop a strategy of summing up the leading logarithmic corrections while accounting for a finite $1/\tau_k$, and derive Eq. (7). The behavior near the edges of the spectral support is discussed in Section V. We compare our findings with the results obtained for the exactly solvable Calogero-Sutherland model in Section VI. Finally, discussion and outlook are presented in Section VII.

II. QUALITATIVE CONSIDERATIONS

In this section we discuss the boundaries (kinematic edges) of the area in (p, ϵ) -plane where the spectral function differs from zero (see Fig. 1). We also provide a simple qualitative framework for understanding the behavior of the spectral function near the kinematic edges and in the vicinity of the particle mass-shell.

A. Support of the spectral function

Using the Lehmann representation, we may express the particle contribution to the spectral function as

$$A_k(\epsilon) \propto \sum_{|f\rangle} |\langle f | \psi_k^{R\dagger} | 0 \rangle|^2 \delta(k - P_{|f\rangle} + P_{|0\rangle}) \delta(\epsilon - E_{|f\rangle} + E_{|0\rangle}). \quad (14)$$

Equation (14) may be viewed as the probability of tunneling of a particle with a given momentum $p_F + k$ and

energy $\epsilon_F + \epsilon$ into a 1D system (to be definite, we consider the right-movers $p_F + k > 0$). The initial state of the transition in Eq. (14) is the ground state of the system $|0\rangle$, and the final state is $|f\rangle$, with $P_{|0\rangle}$, $P_{|f\rangle}$ and $E_{|0\rangle}$, $E_{|f\rangle}$ being the corresponding momenta (relative to p_F) and energies (relative to ϵ_F), respectively.

In the absence of interactions, the only possible final state is that with a single right-moving particle added to the ground state. Because of the momentum conservation the added particle must have momentum k (hereinafter the single-particle momenta are measured relative to the respective Fermi points), $|f\rangle = \psi_{k_F}^{R\dagger} |0\rangle$. Equation (14) then yields $A_k \propto \theta(k) \delta(\epsilon - \xi_k^R)$. With interactions present, states $|f\rangle$ may contain, in addition, a number of particle-hole pairs. This allows $A_k(\epsilon)$ to be finite away from the single-particle mass-shell $\epsilon = \xi_k^R$. Still, there are regions in (p, ϵ) -plane where $A_k(\epsilon) = 0$ due to kinematic constraints. To simplify the analysis of these constraints we focus on the low energies, $|\epsilon| \ll \epsilon_F$, and small momenta $|k| \ll k_F$.

The simplest low-energy final state, beyond the single-particle one, is the state containing one additional particle-hole pair. Given that the total momentum (relative to p_F) is small, the additional pair must have a small momentum too. Therefore, it has to be located in the vicinity of either the right or the left Fermi point. These states, see Figs. 3(a) and 3(b), have the form

$$|f\rangle = \psi_{k_1}^{R\dagger} \psi_{k_2}^{R\dagger} \psi_{k_3}^R |0\rangle, \quad k_1 > 0, \quad k_2 > 0, \quad k_3 < 0 \quad (15)$$

and

$$|f\rangle = \psi_{k_1}^{R\dagger} \psi_{k_2}^{L\dagger} \psi_{k_3}^L |0\rangle, \quad k_1 > 0, \quad k_2 < 0, \quad k_3 > 0, \quad (16)$$

respectively. The state (15) has energy

$$E_{|f\rangle} - E_{|0\rangle} = v(k_1 + k_2 - k_3) + \frac{1}{2m} (k_1^2 + k_2^2 - k_3^2). \quad (17)$$

Taking into account the momentum conservation $k_1 + k_2 - k_3 = k$, we find

$$E_{|f\rangle} - E_{|0\rangle} = vk + \frac{1}{2m} [k_1^2 + k_2^2 - (k_1 + k_2 - k)^2]. \quad (18)$$

The constraints on k_1 , k_2 , and k_3 in Eq. (15) guarantee that $k > 0$. At a given k , the smallest possible value of the excitation energy $E_{|f\rangle} - E_{|0\rangle}$ is reached at $k_1 = k_2 = 0$, $k_3 = -k$.

Similar consideration for the state (16) yields (with momentum conservation $k_1 + k_2 - k_3 = k$ taken into account)

$$E_{|f\rangle} - E_{|0\rangle} = -vk + 2vk_1 - \frac{k^2}{2m} + \frac{k}{m}(k_1 + k_2) - \frac{k_1 k_2}{m}. \quad (19)$$

At $k < 0$, the lowest energy is reached at $k_1 = k_2 = 0$, $k_3 = -k$.

An important observation following from the above analysis is that the lowest possible excitation energy corresponds to the final states with all particles at the Fermi

level, and a *single hole* with the largest possible absolute value of the momentum. It is easy to check that a final state with more than one particle-hole pair excited from the ground state still has the lowest energy when all the available momentum is ‘‘carried’’ by just a single hole. Thus the final states (15) and (16) correspond to the kinematic boundary ξ_k for the particle ($\epsilon > 0$) part of the spectral function. Combining Eqs. (18) and (19) at $k_1 = k_2 = 0$, we find

$$\xi_k = v|k| - k^2/2m. \quad (20)$$

Although we considered here the small- k domain only, Eq. (20) is valid for the entire region $-2p_F < k < 2p_F$, see Fig 1. Finding the spectral edges for higher momenta $|k| > 2p_F$, however, requires consideration of final states with more than one particle-hole pair.

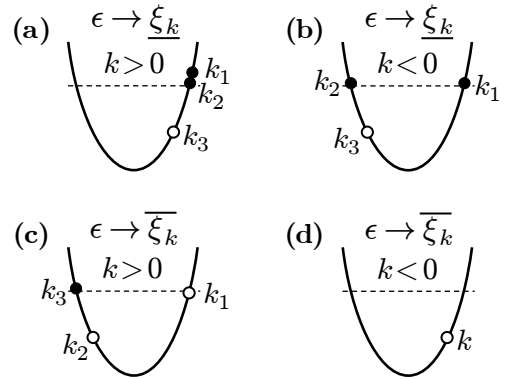


FIG. 3: Final states $|f\rangle$, see Eqs. (14) and (21), corresponding to the boundaries of the regions where $A_k(\epsilon) > 0$. The black (white) circles stand for extra particles (holes) added to the ground state; the dashed line indicates the Fermi level. States (a) and (b) correspond to the particle edge ($\epsilon > 0$); states (c) and (d) correspond to the hole edge.

When considering the hole part of the spectrum, we again start with the Lehmann representation,

$$A_k(\epsilon) \propto \sum_{|f\rangle} |\langle f | \psi_k^R | 0 \rangle|^2 \delta(k + P_{|f\rangle} - P_{|0\rangle}) \delta(\epsilon + E_{|f\rangle} - E_{|0\rangle}). \quad (21)$$

Here $P_{|f\rangle}$ is the momentum of the final state relative to $-p_F$. In the absence of interactions, the matrix element in Eq. (21) is finite only for a single hole excitation with momentum $k < 0$, and $A_k \propto \theta(-k) \delta(\epsilon - \xi_k^R)$. Interaction results in a finite $A_k(\epsilon)$ at $\epsilon \neq \xi_k^R$. Indeed, consider the state [see Fig. 3(c)]

$$|f\rangle = \psi_{k_1}^R \psi_{k_2}^L \psi_{k_3}^{L\dagger} |0\rangle, \quad k_1 < 0, \quad k_2 > 0, \quad k_3 < 0. \quad (22)$$

In zero order in interaction, the energy of this state is

$$E_{|f\rangle} - E_{|0\rangle} = v(-k_1 + k_2 - k_3) - \frac{1}{2m} (k_1^2 + k_2^2 - k_3^2). \quad (23)$$

To find the spectral edge [i.e., the largest possible value of ϵ in Eq. (21) at a given k], we look for the lowest possible energy of the final state $E_{|f\rangle}$ in Eq. (23). Given

the momentum conservation, $k_1 + k_2 - k_3 = k$, this limit is reached at $k_1 = k$, $k_2 = k_3 = 0$ for $k < 0$, and at $k_2 = k$, $k_1 = k_3 = 0$ for $k > 0$. In other words, the lowest-energy final state (hence the highest possible ϵ) coincides with the energy of a single hole, see Figs. 3(c) and 3(d). Consideration of final states with more than one particle-hole pair excited does not change this conclusion. Accordingly, the kinematic boundary for the hole part of the spectral function at small k is given by

$$\overline{\xi}_k = -v|k| + k^2/2m. \quad (24)$$

Just as it is the case for $\epsilon > 0$, Eq. (24) is valid for $|k| < 2p_F$; finding the kinematic boundary for higher momenta requires consideration of final states with more excitations.

The support of the spectral function in (p, ϵ) -plane is illustrated in Fig. 1.

B. Spectral function near the edges of the support

Near the edges of support in (p, ϵ) -plane, the spectral function displays a power-law dependence on the distance to the edge. The behavior of $A_k(\epsilon)$ near the hole mass-shell,

$$A_k(\epsilon) \propto (\overline{\xi}_k - \epsilon)^{\gamma_k^2 - 1} \theta(\overline{\xi}_k - \epsilon), \quad -2p_F < k < 0, \quad (25)$$

is very similar to that in the TL model. The deviation of the exponent in Eq. (25) from (-1) is quadratic in the interaction and positive, just like it is in the TL model.

Adding an extra hole to an interacting system is accompanied by the creation of “soft” particle-hole pairs; we considered an example of such three-particle final state in the previous subsection, see Eq. (22) and Fig. 3(c). Excitation of multiple low-energy particle-hole pairs leads to the orthogonality catastrophe²², thus the correction to (-1) in the exponent is positive and is proportional to γ_k^2 . The main difference compared with the TL model is that now the extra hole interacts with the soft pairs residing near both Fermi points, while in the TL model only pairs on the opposite branch of the spectrum contribute to the singularity.

When the edge of the spectral support no longer coincides with the mass-shell, which is always the case for particles ($\epsilon > 0$) and at $0 < k < 2p_F$ also for holes ($\epsilon < 0$), the behavior of the spectral function near the edge is different from that described by Eq. (25). We find that the corresponding exponents are *positive* and finite even in the limit $\gamma_k \rightarrow 0$.

To be definite, let us consider the particle edge $\epsilon \rightarrow \underline{\xi}_k$ at $k < 0$. The spectral function differs from zero in the vicinity of the edge due to three-particle final states $|f\rangle = \psi_{k_1}^{R\dagger} \psi_{k_2}^{L\dagger} \psi_{k_3}^L |0\rangle$, see Eq. (16) and Fig. 3(b). If we replace the matrix element in Eq. (14) by a constant, then the dependence of $A_k(\epsilon)$ on $\epsilon - \underline{\xi}_k$ can be found by

power counting,

$$\begin{aligned} A_k(\epsilon) &\propto \int dk_1 dk_2 dk_3 \delta(k_1 + k_2 - k_3 - k) \\ &\quad \times \delta(\epsilon - \xi_{k_1}^R - \xi_{k_2}^L + \xi_{k_3}^L) \\ &\propto (\epsilon - \underline{\xi}_k) \theta(\epsilon - \underline{\xi}_k). \end{aligned} \quad (26)$$

Eq. (26) corresponds to the final state $|f\rangle$ with two particles close to the Fermi points $\pm p_F$ and a “deep” hole with momentum (relative to $-p_F$) approaching k , see Fig. 3(b). Interaction of the two particles near the Fermi level with the hole and with each other leads to a logarithmic renormalization of the matrix element in Eq. (14). Similar to the X-ray edge singularity problem²³, the renormalization occurs already in the first order in the interaction strength and leads to

$$A_k(\epsilon) \propto (\epsilon - \underline{\xi}_k)^{1 - \mu_k - \mu_{2p_F+k} + 2\mu_{2p_F}}, \quad -2p_F < k < 0. \quad (27)$$

For a short range interaction and small momenta $|k| \ll p_F$ we have $\mu_k \ll \mu_{2p_F} = 2\gamma_0$, and Eq. (27) simplifies to

$$A_k(\epsilon) \propto (\epsilon - \underline{\xi}_k)^{1+2\gamma_0}.$$

For a linear spectrum (TL model), the left-moving particle and hole have the same velocity, destroying the core-hole effect leading to Eq. (27).

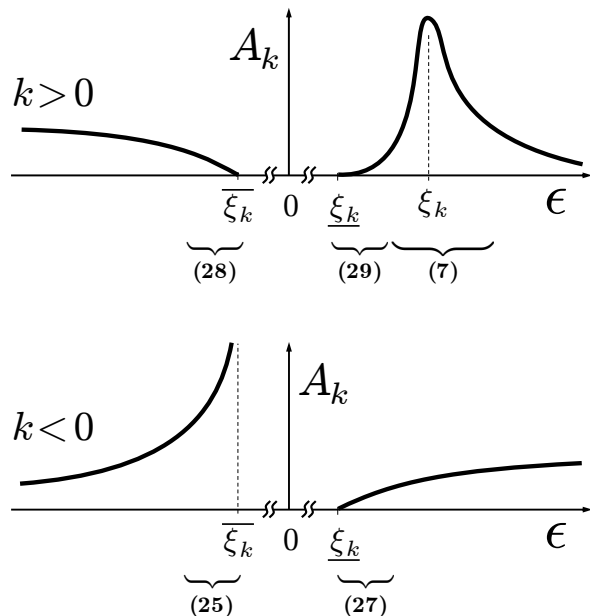


FIG. 4: Dependence of the spectral function on ϵ at a fixed $k = p - p_F$ with $k > 0$ (upper panel) and $k < 0$ (lower panel). The numbers in brackets refer to the equations describing the corresponding asymptotes of $A_k(\epsilon)$. At large $|\epsilon - \underline{\xi}_k|, |\epsilon - \overline{\xi}_k| \gg k^2/m$ (this region is not shown in the figure) the conventional Luttinger liquid behavior $A_k(\epsilon) \propto |\epsilon + vk|^{\gamma_0^2} |\epsilon - vk|^{\gamma_0^2 - 1}$ is restored.

The consideration of spectral function near the hole

edge $\epsilon \rightarrow \bar{\xi}_k$ at $k > 0$ is very similar, yielding

$$A_k(\epsilon) \propto (\bar{\xi}_k - \epsilon)^{1-2\mu_{2p_F} - \mu_k + \mu_{2p_F - k}}, \quad 0 < k < 2p_F. \quad (28)$$

The signs of two terms in the exponent here are different from those in Eq. (27) because of the difference in the structure of the relevant final states. In the three-body sector, for example, the final state consists of one particle and two holes (rather than two particles and one hole as in the case of Eq. (27) above), see Fig. 3(c). For a short-range interaction and small momenta, Eq. (28) simplifies to

$$A_k(\epsilon) \propto (\bar{\xi}_k - \epsilon)^{1-2\gamma_0}.$$

Finally, we discuss the particle edge $\epsilon \rightarrow \underline{\xi}_k$ at $k > 0$. A new element here is that the relevant soft excitations reside on the same branch of the spectrum. When ϵ is close to $\underline{\xi}_k$, these excitations tend to occupy almost identical right-moving states with $k \rightarrow 0$. In the specific example of the final state shown in Fig. 3(a), the momenta of two particles differ by $\sim (\epsilon - \underline{\xi}_k)/v$. This results in a suppression of the matrix element in Eq. (14), $|\langle f | \psi_k^{R\dagger} | 0 \rangle| \propto \epsilon - \underline{\xi}_k$. A proper modification of Eq. (26) then leads to $A_k(\epsilon) \propto (\epsilon - \underline{\xi}_k)^3$. Accounting for the particle-hole interaction in the final state yields

$$A_k(\epsilon) \propto (\epsilon - \underline{\xi}_k)^{3-2\mu_k}, \quad 0 < k < 2p_F. \quad (29)$$

At $k = 2p_F$ (i.e. $p = 3p_F$) the spectral edge $\underline{\xi}_k$ touches zero, $\underline{\xi}_{2p_F} = 0$. Close to this point the exponent can be evaluated using the conventional bosonization technique²⁴. It yields $3 - 4\gamma_0$ for the exponent in agreement with Eq. (29) (indeed, $\mu_{2p_F} = 2\gamma_0$).

The dependence of the spectral function on ϵ at a fixed k is sketched in Fig. 4.

C. Spectral function near the particle mass-shell

For a nonlinear spectrum (6) the particle mass-shell $\epsilon = \xi_k^R > 0$ lies *above* the lower edge of the spectral support, $\underline{\xi}_k = \xi_k^R - k^2/m$. Far away from the mass-shell the difference between ξ_k^R and $\underline{\xi}_k$ is not important, and at $\epsilon - \xi_k^R \gg k^2/m$ the spectral function $A_k(\epsilon)$ approaches the TL form Eq. (4). In the vicinity of the mass-shell, however, $A_k(\epsilon)$ undergoes a dramatic change. Indeed, since $\epsilon = \xi_k^R$ now lies within a broader continuum, the quasiparticle relaxation (decay) is no longer prohibited by the conservation laws. As a result, in a parametrically wide region (indicated by dark gray in Fig. 1) the quasiparticle peak in $A_k(\epsilon)$ acquires a Fermi-liquid-like Lorentzian shape, see Eq. (11).

It is instructive to discuss the origin of a finite relaxation rate in a 1D Fermi system. First of all, unlike in higher dimensions, relaxation in 1D can not occur via two-particle collisions. Indeed, conservation of the momentum and energy allows at most a *permutation* of the momenta of two colliding particles.

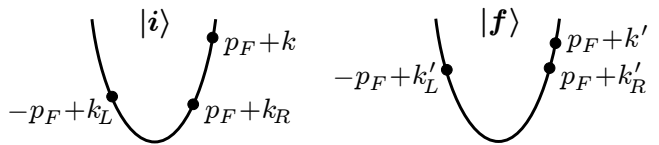


FIG. 5: The initial (left panel) and the final (right panel) states of a three-particle scattering process that leads to a quasiparticle relaxation in one dimension.

Scattering processes that result in a *redistribution* of the momenta and thus potentially lead to a finite relaxation rate must involve at least three particles. In such three-body collision three particles with momenta k , k_R , and k_L (relative to $\pm p_F$) in the initial state $|i\rangle$ end up in a final state $|f\rangle$ with *different* momenta k' , k'_R , and k'_L , see Fig. 5. For a *generic* interaction²¹ the transition $|i\rangle \rightarrow |f\rangle$ has a nonvanishing amplitude \mathcal{A} .

In order to estimate the relaxation rate of an extra right-moving particle with momentum k due to three-body collisions, we note that the single-particle states k_R, k_L in the initial state of the transition $|i\rangle$ are below the Fermi level, while all three single-particle states in the final state $|f\rangle$ are above it. Applying now the Golden Rule, we find

$$\begin{aligned} \frac{1}{\tau_k} &\propto \int_0^\infty dk' dk'_R dk_L \int_{-\infty}^0 dk'_L dk_R |\mathcal{A}|^2 \\ &\times \delta[(k + k_R + k_L) - (k' + k'_R + k'_L)] \\ &\times \delta\left[\left(\xi_k^R + \xi_{k_R}^R + \xi_{k_L}^L\right) - \left(\xi_{k'}^R + \xi_{k'_R}^R + \xi_{k'_L}^L\right)\right], \end{aligned} \quad (30)$$

where \mathcal{A} is the three-body collision amplitude introduced above, and the δ -functions express the energy and momentum conservation.

In writing Eq. (30) we took into account that for $k \ll p_F$ the conservation laws cannot be satisfied unless the collision involves both the right- and the left-moving particles. Further analysis shows that the conservation laws allow a small ($\lesssim k^2/m$) momentum transfer to the left-movers. Such solution can be found by iterations. To zero order in $k_L - k'_L$, the momentum conservation gives $k - k' = k'_R - k_R$. The energy released in the collision of two right-moving particles then is $\xi_k^R + \xi_{k_R}^R - \xi_{k'}^R - \xi_{k'_R}^R \lesssim k^2/m$. This energy is transferred to the left-movers, $\xi_{k'_L}^L - \xi_{k_L}^L \lesssim k^2/m$, which corresponds to the momentum transfer $k_L - k'_L \lesssim k^2/mv \ll k$. Accordingly, the energy and momentum conservation restrict the range of the momenta contributing to the integral in Eq. (30) to

$$k', k'_R, |k_R| \lesssim k, \quad k_L, |k'_L| \lesssim k^2/mv. \quad (31)$$

The δ -functions in Eq. (30) remove the integrations over k'_R and k'_L . With the phase space constraints (31) taken into account, the remaining integrations then yield the estimate

$$1/\tau_k \propto |\mathcal{A}|^2 k^4. \quad (32)$$

For a weak generic²¹ interaction, the nonvanishing 3-particle collision amplitude \mathcal{A} appears in the second order in the interaction strength. More careful consideration (see Section III) which accounts for the indistinguishability of the two right-moving particles participating in the collision results in the estimate

$$\mathcal{A} \propto V_0(V_0 - V_k) \propto k^2, \quad (33)$$

cf. Eq. (10). Accordingly, the quasiparticle decay rate scales with k as $1/\tau_k \propto k^8$.

III. PERTURBATION THEORY

In this section we evaluate the imaginary part of the self-energy $\text{Im} \Sigma_p(\epsilon)$ perturbatively in the interaction strength. Specifically, we focus on the near vicinity of the mass-shell $\epsilon \approx \xi_p$. The Fermi liquid theory predicts a nonzero self-energy already in the second order in the interaction strength, see Eq. (2). We show below that in one dimension the second-order contribution to $\text{Im} \Sigma_p(\epsilon)$ vanishes on the mass-shell, even if the curvature of the dispersion relation Eq. (6) is taken into account. A finite quasiparticle decay rate appears only in the fourth order, and only if $m^{-1} \neq 0$.

We describe interacting spinless fermions by the Hamiltonian

$$H = \sum_{\alpha,k} \xi_k^\alpha \psi_k^{\alpha\dagger} \psi_k^\alpha + \frac{1}{2L} \sum_{q \neq 0} [V_q \sum_\alpha \rho_q^\alpha \rho_{-q}^\alpha + 2U_q \rho_q^R \rho_{-q}^L], \quad (34)$$

where $\alpha = R, L$, the dispersion relation ξ_k^α is given by Eq. (6), and $\rho_q^\alpha = \sum_k \psi_{k-q}^{\alpha\dagger} \psi_k^\alpha$ is the Fourier component of the density operator. We found it convenient to distinguish between the interbranch and the intrabranched interaction potentials (denoted by U_q and V_q , respectively)²¹. However, for the sake of brevity, we will set $U_q = V_q$ in the results.

A. Second order

Evaluation of the self-energy in the second order of perturbation theory at $|\epsilon| > |\xi_p|$ parallels the corresponding calculation in the problem with linear dispersion relation (Tomonaga-Luttinger model). The only finite contribution comes from the interbranch interaction U , and the result reads

$$-\text{Im} \Sigma_p^{(2)}(\epsilon) = \gamma_0^2 (\epsilon - \xi_p) \left[\frac{1}{\pi} \ln \frac{|\epsilon^2 - \xi_p^2|}{\epsilon_F^2} + i\theta(|\epsilon| - |\xi_p|) \right] \quad (35)$$

with $\gamma_0 = \nu U_0/2$. Vanishing of the imaginary part of the self-energy below the mass-shell is due to kinematic constraints: the phase space available for scattering process vanishes in the limit $\epsilon \rightarrow \xi_p$.

For $|\epsilon| < |\xi_p|$ real decay processes are allowed by conservation laws only if the dispersion is nonlinear. For

clarity, we consider the decay of a right-moving particle ($\xi_k^R > 0$). In the presence of the spectrum nonlinearity $\text{Im} \Sigma_k$ acquires an additional contribution in the second order in the intrabranched interaction V . This contribution comes from the scattering processes with two particles and one hole in the final state, all three on the right moving branch. The Golden-rule expression for $\text{Im} \Sigma_k$ reads

$$-\text{Im} \Sigma_k^{(2)}(\epsilon) = \frac{\pi}{2} \sum_{k_1, k_2} \left| \mathcal{A}_V^{(1)} \right|^2 \delta(\epsilon - \xi_{k_1}^R - \xi_{k_2}^R + \xi_{k_3}^R), \quad (36)$$

where $k = p - p_F$ and $k_1 + k_2 - k_3 = k$ due to momentum conservation. The Fermi statistics dictates that $k_1, k_2 > 0$ and $k_3 < 0$. The amplitude of the scattering process is given by

$$\mathcal{A}_V^{(1)} = V_{k-k_1} - V_{k-k_2}. \quad (37)$$

The conservation laws are satisfied only in the limited energy range, $\xi_k \leq \epsilon \leq \xi_k^R$ with $\xi_k = \xi_k^R - k^2/m$, see Eq. (20). We defer the discussion of the spectral function near the lower edge of the spectrum $\epsilon = \xi_k$ to Section V, and focus here on the immediate vicinity of the mass-shell, $|\epsilon - \xi_k^R| \ll k^2/2m$. In this limit Eq. (36) yields

$$-\text{Im} \Sigma_k^{(2)}(\epsilon) = \frac{\mu_k^2}{4} (\xi_k^R - \epsilon) \theta(\xi_k^R - \epsilon) \quad (38)$$

with μ_k defined in Eq. (9) and ξ_k^R given by Eq. (6). The real part of the self-energy is given by

$$-\text{Re} \Sigma_k^{(2)}(\epsilon) = \frac{\mu_k^2}{4\pi} (\epsilon - \xi_k^R) \ln \frac{|\epsilon - \xi_k^R|}{k^2/m}. \quad (39)$$

According to Eq. (38), the intrabranched interaction along with the positive curvature of the dispersion relation ($1/m > 0$) results in a finite $\text{Im} \Sigma_k^{(2)}$ at $\epsilon < \xi_k^R$. Eq. (38) complements Eq. (35), familiar from the conventional TL theory. Note that in both cases $\text{Im} \Sigma_k^{(2)}(\epsilon)$ vanishes on the mass-shell due to the phase space constraints.

For the particle branch of spectrum ($\epsilon \approx \xi_k^R > 0$), the kinematic restrictions on the phase space are lifted in higher-order processes. The simplest process leading to a finite self-energy on the mass-shell is the second-order process that results in the creation of two particle-hole pairs in the final state.

B. Fourth order

There are two kinds of the fourth order processes. The first one leads to a logarithmic correction to the scattering amplitude via virtual creation of a particle-hole pair. Similar logarithmic corrections appear in higher orders of perturbation theory as well. Summation of the leading logarithmic contributions in all orders (the corresponding

procedure is described in Section IV) results in a power-law behavior of the spectral function. This is very similar to the TL model, although with the exponent slightly modified due to the dispersion nonlinearity.

A different kind of second-order processes, leading to the finite on-shell value of $\text{Im} \Sigma_k$, involve creation of five

quasiparticles in the final state: a particle on the right-moving branch, and two particle-hole pairs. Kinematic considerations show that the two pairs must be excited on the opposite branches of the spectrum in order to yield $\text{Im} \Sigma_k \neq 0$ on the shell. The corresponding contribution to the self-energy is then given by

$$-\text{Im} \Sigma_k^{(4)}(\epsilon) = \frac{\pi}{2} \sum_{q, Q, k_1, k_2} \left| \mathcal{A}^{(2)} \right|^2 \delta(\epsilon - \xi_{k-q+Q}^R + \xi_{k_1-q}^R - \xi_{k_1}^R - \xi_{k_2-Q}^L + \xi_{k_2}^L), \quad (40)$$

where the summation range is limited by the Pauli principle constraints

$$k - q + Q, k_1, k_2 > 0; \quad k_1 - q, k_2 - Q < 0,$$

and the amplitude $\mathcal{A}^{(2)}$ consists of two contributions,

$$\mathcal{A}^{(2)} = \mathcal{A}_{UU}^{(2)} + \mathcal{A}_{UV}^{(2)}. \quad (41)$$

These two contributions correspond to two possible ways the desired final state can be reached in a second-order process: The first one, $\mathcal{A}_{UU}^{(2)} \propto U^2$, arises solely due to the interbranch interaction U , see Fig. 6. The second one, $\mathcal{A}_{UV}^{(2)} \propto UV$, involves both the interbranch (U) and the intrabranched (V) interactions, see Fig. 7. The corresponding analytical expressions read

$$\mathcal{A}_{UU}^{(2)} = \frac{U_q U_{q-Q}}{\xi_{k_1}^R - \xi_{k_1-q}^R + \xi_{k_2-Q}^L - \xi_{k_2+q-Q}^L} + \frac{U_q U_{q-Q}}{\xi_{k_1-q}^R - \xi_{k_1}^R + \xi_{k_2}^L - \xi_{k_2-Q}^L} - \frac{U_{k-k_1+Q} U_{k-k_1}}{\xi_{k-q+Q}^R - \xi_{k_1-q}^R + \xi_{k_2-Q}^L - \xi_{k_2+k-k_1}^L} - \frac{U_{k-k_1+Q} U_{k-k_1}}{\xi_{k_1-q}^R - \xi_{k-q+Q}^R + \xi_{k_2}^L - \xi_{k_2-Q+k_1-k}^L}. \quad (42)$$

$$\mathcal{A}_{UV}^{(2)} = \frac{U_Q (V_{q-Q} - V_{k-k_1+Q})}{\xi_{k_1}^R - \xi_{k_1-Q}^R - \xi_{k_2}^L + \xi_{k_2-Q}^L} + \frac{U_Q (V_{q-Q} - V_{k-k_1})}{\xi_{k_1-q}^R - \xi_{k_1-q+Q}^R + \xi_{k_2}^L - \xi_{k_2-Q}^L} + \frac{U_Q (V_q - V_{k-k_1})}{\xi_{k-q+Q}^R - \xi_{k-q}^R - \xi_{k_2}^L + \xi_{k_2-Q}^L} + \frac{U_Q (V_q - V_{k-k_1+Q})}{\xi_{k-q+Q}^R - \xi_{k_1-q}^R + \xi_{k_1}^R - \xi_{k+Q}^R}. \quad (43)$$

(A more general but rather cumbersome expression for the amplitude free from the simplifying assumption [21] is derived in Ref. [25].)

One immediately notices that $\mathcal{A}_{UV}^{(2)}$ vanishes for the momentum-independent intrabranched interaction $V_q = V_0$. Although it is not obvious, the amplitude $\mathcal{A}_{UU}^{(2)}$ vanishes²⁶ for momentum-independent interbranch interactions $U_q = U_0$ and for a strictly parabolic dispersion relation.

To proceed further, we assume that both inter- and intrabranched interactions are symmetric analytic functions of the transferred momentum; at small momenta

$$U_q \approx U_0 + \frac{1}{2} U_0'' q^2, \quad V_q \approx V_0 + \frac{1}{2} V_0'' q^2, \quad (44)$$

and at large q the potentials vanish sufficiently fast²¹. We also neglect cubic and higher-order terms in the dispersion relation Eq. (6).

We will evaluate Eq. (40) for $\epsilon = \xi_k^R$. In this limit the typical momentum of the right-moving particles in the final states contributing to $\text{Im} \Sigma_k^{(4)}$ is of the order of k and the velocity variation is $\sim k/m$. The energy gain due to the production of the right-moving particle-hole pairs is therefore $\sim k(k/m)$. Conservation of energy then yields the estimate for the typical momenta of the left-moving particle and hole in the final state,

$$k_2 \sim Q \sim k^2/mv \ll k.$$

Carrying out the summation over k_1 in Eq. (40), we obtain

$$-\text{Im} \Sigma_k^{(4)}(\xi_k^R) = \sum_{q, Q} \sum_{0 < k_2 < Q} \frac{m}{4q} \left| \mathcal{A}^{(2)} \right|^2, \quad (45)$$

where the summations over q and Q are restricted to the

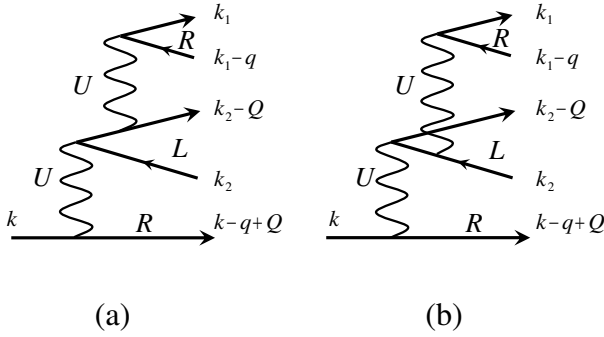


FIG. 6: Second order in U contributions to the amplitude $\mathcal{A}_{UU}^{(2)}$. (a) and (b) correspond, respectively, to the first and second terms in Eq. (42). Two more contributions (not shown in the figure) correspond to the replacement $k_1 \leftrightarrow k - q + Q$ in the final states; these are the third and the fourth terms in Eq. (42).

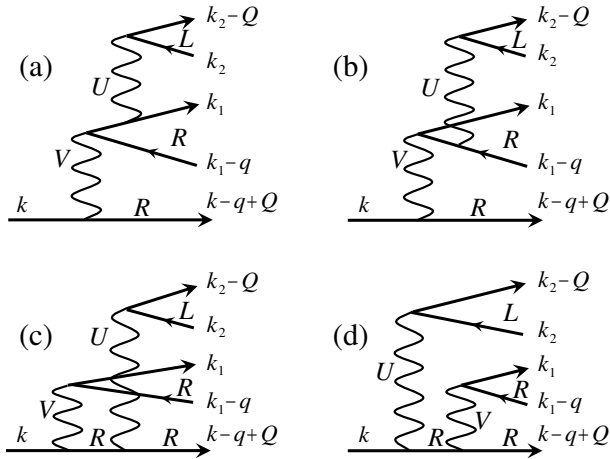


FIG. 7: Second order contributions to the amplitude $\mathcal{A}_{UV}^{(2)}$. (a)-(d) correspond to the first terms in the numerators of the four contributions in Eq. (43). Four more contributions (not shown in the figure) correspond to the replacement $k_1 \leftrightarrow k - q + Q$ in (a)-(d).

domain

$$0 < q < k, \quad \frac{(k-q)q}{2mv} < Q < \frac{kq}{2mv}. \quad (46)$$

The amplitude $\mathcal{A}^{(2)}$, see Eqs. (41)-(43), simplifies considerably in the limit $k \ll mv$. Keeping only linear in U_0'' and V_0'' contributions, we find

$$\mathcal{A}^{(2)} = U_0 (2U_0'' + V_0'') \frac{q^4 - (2mvQ)^2}{8mv^2q^2}. \quad (47)$$

The high powers of the momenta here as well as the factor $1/m$ resulted from delicate cancellations among various contributions to the amplitude. Since the amplitude (47) is independent of k_2 , the integration over this variable in Eq. (40) brings about a factor $Q/2\pi$. The remaining

integration over q and Q is restricted to the domain D defined in Eq. (46),

$$-\text{Im} \Sigma_k^{(4)}(\xi_k^R) = \int_D \frac{dq dQ}{4\pi^2} \frac{mQ}{8\pi q} |\mathcal{A}^{(2)}|^2$$

The integration here is straightforward and yields

$$-\text{Im} \Sigma_k^{(4)}(\xi_k^R) = \frac{3U_0^2 (2U_0'' + V_0'')^2 k^8}{5(32\pi m v^2)^3}. \quad (48)$$

Note that $\text{Im} \Sigma_k^{(4)}(\xi_k^R)$ scales with k as k^8 . The factor k^4 here originates in the amplitude: according to Eq. (47), its typical value is $\mathcal{A}^{(2)} \propto k^2$. The remaining factor k^4 comes from the integration over Q (recall that $Q \propto k^2$). Using now $k^2 V_0'' \approx 2(V_k - V_0)$, see Eq. (44), and setting $U_k = V_k$, we arrive at Eq. (10) with $1/2\tau_k = -\text{Im} \Sigma_k^{(4)}(\xi_k^R)$ [here we took into account that $\text{Im} \Sigma_k^{(2)}(\xi_k) = 0$].

The above derivation can be extended to $\epsilon \neq \xi_k^R$. The self-energy varies with ϵ on the scale of the order of $k^2/2m$, and it vanishes identically for $\epsilon < \xi_k$, as expected from the kinematic considerations of Section II.

According to the developed perturbation theory the spectral function in the vicinity of the particle mass-shell takes the form

$$A_k(\epsilon) = \frac{1}{\pi} \frac{-\text{Im} \Sigma_k(\epsilon)}{(\epsilon - \xi_k^R)^2 + [\text{Im} \Sigma_k(\epsilon)]^2}, \quad (49)$$

where $\Sigma_k(\epsilon) = \Sigma_k^{(2)}(\epsilon) + \Sigma_k^{(4)}(\epsilon)$ and the corresponding contributions are given by Eqs. (35), (38), and (48). As a result, the spectral function in the energy interval

$$-(\tau_k \mu_k^2)^{-1} \lesssim \epsilon - \xi_k^R \lesssim (\tau_k \gamma_0^2)^{-1}$$

around the mass-shell is a Lorentzian with the width $1/2\tau_k$. Outside this interval $\text{Im} \Sigma_k^{(2)}(\epsilon) > \text{Im} \Sigma_k^{(4)}(\epsilon)$ and the spectral function is described by a power law $A_k(\epsilon) \sim |\epsilon - \xi_k^R|^{-1}$, with the exponent equal to (-1) . The perturbation theory developed so far does not take into account the logarithmic renormalization of the scattering amplitudes. In Section IV we show that summation of the leading logarithmic corrections leads to the interaction-dependent correction to the exponent. The height of the Lorentzian peak Eq. (49), is also renormalized, see Eq. (11) above.

IV. LEADING LOGARITHMIC CORRECTIONS

It is easy to see that excitation of virtual particle-hole pairs leads to the logarithmically divergent contributions in perturbation theory, in a very much the same way as in the TL model. The real part of the self-energy acquires such logarithmic corrections already in the second order in interaction, see Eq. (35). The logarithmic terms in the imaginary part of the self-energy appear in the fourth

order. [These contributions vanish on the mass-shell, and thus do not affect the validity of Eq. (48)].

In this section we develop a procedure for the summation of the leading logarithmic corrections to the Green function $G_k(\epsilon)$ in the presence of nonlinear terms in the dispersion relation Eq. (6). The nonlinearity is not important as long as $|\epsilon - \xi_k^R| \gg k^2/2m$. Close to the mass-shell, however, the behavior of the spectral function deviates significantly from that in the conventional Luttinger liquid. For a positive curvature [i.e. for $1/m > 0$ in Eq. (6)], deviations are the strongest for the particle ($\epsilon > 0$) excitations with $k > 0$; we have already seen that the on-shell excitations acquire a finite lifetime τ_k . On the other hand, the behavior of the hole branch ($\epsilon < 0$) is qualitatively similar to that of a Luttinger liquid. We will concentrate here on the properties of the particle branch at $|\epsilon - \xi_k| \ll k^2/m$, deferring the discussion of the hole region of the spectrum till the end of this Section.

A. Vicinity of the particle mass-shell: $\epsilon \rightarrow \xi_k^R$, $k > 0$

In order to account simultaneously for both the logarithmic renormalization and the finite quasiparticle lifetime, we notice that the relevant energy scales form a well-defined hierarchy

$$\frac{1}{2\tau_k} \ll \frac{k^2}{2m} \ll \xi_k^R \ll mv^2. \quad (50)$$

The logarithmic corrections originate from almost the entire energy band, i.e. from the states with energies in the range $(|\epsilon - \xi_k^R|, mv^2)$. On the other hand, the finite lifetime $1/\tau_k$ originates in the decay of a particle into particle and hole states within much narrower strip of energies of the width of the order of ξ_k^R .

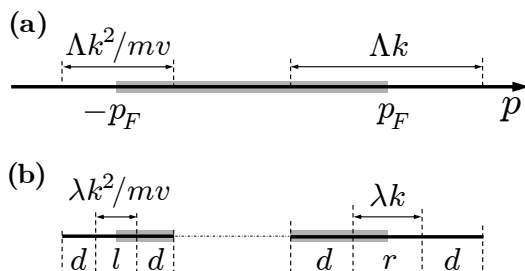


FIG. 8: (a) Subbands in the momentum space remaining after performing the RG transformation described in step (i) in the text. (b) Subbands of the effective model described by the Hamiltonian (58). The state with $k > 0$ under consideration belongs to d -subband.

Our strategy for evaluation of the Green function will be as follows:

(i) First we will take into account virtual transitions to states with relatively high energies, corresponding to the momenta p in the range $\Lambda k \lesssim |p - p_F| \lesssim p_F$ for the right-movers and $\Lambda k^2/mv \lesssim |p + p_F| \lesssim p_F$ for the

left-movers (here $\Lambda \gg 1$). This step is similar to the standard renormalization group (RG) calculation for the Tomonaga-Luttinger model²⁷. As a result of “integrating out” the high-energy states, $G_k(\epsilon)$ acquires a multiplicative factor. In addition, some irrelevant terms are generated in the Hamiltonian; these terms do not affect the logarithmic renormalization of $G_k(\epsilon)$, but contribute to the decay rate $1/\tau_k$ which is evaluated on the latter stage. The multiplicative RG terminates when the energy bands have been reduced to strips of the right-moving states with $|p - p_F| \lesssim \Lambda k$, and the left-movers with $|p + p_F| \lesssim \Lambda k^2/mv$, see Fig. 8(a).

(ii) In the next step, we separate the remaining states in three groups. The first two (subbands r and l) correspond to two segments, $|p - p_F| \lesssim \lambda k$ and $|p + p_F| \lesssim \lambda k^2/mv$ on the right- and left-moving branches, respectively; hereinafter $\lambda \ll 1$. The rest of the states form subbands d , see Fig. 8(b). The state of interest k belongs to the right-moving branch of d -subband. This state acquires a finite lifetime τ_k , which manifests itself in the shifting of the pole in $G_k(\epsilon)$ by $i/2\tau_k$ off the real axis. Importantly, the dominant contribution to the finite lifetime comes from the decay of the state of interest into other states within d -band. Although the subbands r and l make a negligible contribution to the decay rate $1/\tau_k$, the density fluctuations in these subbands induce a slowly varying [on the timescale of the order of $(k^2/2m)^{-1}$] fluctuating field that affects the dynamics of the high-energy ($\epsilon \sim \xi_k^R$) d -particle. Our formalism accounts for both these fluctuations and for the finite decay rate $1/2\tau_k$, and leads to Eq. (7).

Now we sketch the implementation of the two steps described above. (Some technical details are relegated to Appendixes A and B.)

Step (i) follows, with a small modification, the conventional RG procedure employed in the theory of Tomonaga-Luttinger model²⁷. We introduce a reduced space of single-particle states with $|p - p_F| < k_R$ for the right-movers and $|p + p_F| < k_L$ for the left-movers and consider the Green function, $G_k(\epsilon; k_L, k_R)$, defined in the reduced band. Following the idea of the multiplicative RG²⁷, we consider the transformation of the Green function associated with the reduction of the bandwidth ($k_L \rightarrow k'_L$, $k_R \rightarrow k'_R$), and cast it in the form

$$G_k(\epsilon; k'_L, k'_R) = z \left(\frac{k'_L}{k_L}, \frac{k'_R}{k_R} \right) G_k(\epsilon; k_L, k_R) \quad (51)$$

Next, we use the results of the Section III A to evaluate the Green function (51) perturbatively in the second order in the interaction potential. This leads to an approximate expression for z ,

$$z \left(\frac{k'_L}{k_L}, \frac{k'_R}{k_R} \right) = 1 - 2\gamma_0^2 \cdot \ln \frac{k'_L}{k_L} - 0 \cdot \ln \frac{k'_R}{k_R}, \quad (52)$$

where $\Lambda k < k'_{L,R} < p_F$. The last term on the right-hand side here expresses the fact that the renormalization of $G_k(\epsilon)$ for a right-mover results from its interaction with the left-movers; this is why the function z

depends only on a single argument k'_L/k_L . Eq. (52) is valid up to the second order in γ_0 , and also assumes that $\gamma_0^2 \ln(k'_L/k_L) \ll 1$. In order to find $z(k'_L/k_L)$, we supplement Eq. (52) by the requirement that the scaling function has a multiplicative property²⁷. That leads to

$$z\left(\frac{k'_L}{k_L}, \frac{k'_R}{k_R}\right) = \left(\frac{k'_L}{k_L}\right)^{-2\gamma_0^2}, \quad \Lambda k < k_{R,L}, k'_{R,L} < p_F. \quad (53)$$

In order to keep the state of interest k under consideration it must lie within the reduced band of right-movers. Accordingly, the scaling of the right band must stop at $k'_R \approx \Lambda k$. However, the bandwidth of the left-movers can be reduced even further, all the way down to $k'_L \approx \Lambda k^2/mv$. The latter scale represents the width of the band to which the states involved in real transitions associated with the formation of $1/\tau_k$ belong, see Section III B. (Note that according to Eq. (35), the scaling exponent in the interval $\Lambda k^2/mv < k'_L < \Lambda k$ is γ_0^2 rather than $2\gamma_0^2$).

Using now Eqs. (51) and (53), we find

$$G_k(\epsilon) = \left(\frac{\Lambda kv}{\epsilon_F}\right)^{2\gamma_0^2} \left(\frac{\Lambda k^2/m}{\Lambda kv}\right)^{\gamma_0^2} G_k\left(\epsilon; \frac{\Lambda k^2}{mv}, \Lambda k\right) \quad (54)$$

(we used $mv \sim p_F$ here). Note that the nonlinearity of the single-particle spectrum does not affect the form of Eqs. (52) and (54) as long as $\Lambda \gg 1$.

However, because of the nonlinearity, reduction of the bandwidth ($k_F \rightarrow \Lambda k^2/p_F$) generates an additional interaction term

$$\hat{V}_\Lambda = \sum M \psi_{k_1}^{R\dagger} \psi_{k-q-Q}^{R\dagger} \psi_{k_2-Q}^{L\dagger} \psi_{k_2}^L \psi_k^R \psi_{k_1-q}^R. \quad (55)$$

The matrix element M here accounts for the contributions to the total transition amplitude $\mathcal{A}^{(2)}$ of the virtual states outside the reduced band of the left-movers. These states contribute to $\mathcal{A}_{UV}^{(2)}$, but not to $\mathcal{A}_{UV}^{(2)}$. Therefore one finds $M \approx (1/2)\mathcal{A}_{UV}^{(2)}$ (here 1/2 is a combinatorial factor). Since all the momenta in Eq. (55) belong to the reduced band, we have

$$M = U_0 U_0'' \frac{q^4 - (2mvQ)^2}{8mv^2q^2}. \quad (56)$$

as it is clear from the analysis leading to Eq. (47). Using $q \sim k$ and $Q \sim k^2/p_F$, we estimate $M \sim k^2/mv^2$, i.e., M vanishes for a linear spectrum. The generated interaction Eq. (55) is to be added to the Hamiltonian Eq. (34), where all the operators now act within the band of reduced width. Along with the interaction terms already present in Eq. (34), \hat{V}_Λ contributes to the inelastic scattering processes giving rise to a finite quasiparticle relaxation rate $1/\tau_k$.

We now proceed to step (ii) of the program outlined above, i.e., evaluation of the Green function in the reduced band. To this end, we separate the states in the reduced band in two narrow subbands: the l -band with

$|k^*| \lesssim \lambda k^2/p_F$ around the left Fermi point, and the r -band with $|k^*| \lesssim \lambda k$ around the right Fermi point. The remaining states form subband d , see Fig. 8(b). Parameter λ here satisfies the conditions

$$\gamma_0^2 \ln \frac{\Lambda}{\lambda} \ll 1, \quad \lambda \ll 1. \quad (57)$$

(Note that at $\gamma_0 \ll 1$ the two conditions (57) can be satisfied simultaneously.) The states within the subbands r and l produce additional logarithmic renormalization of the Green function. The first condition in Eq. (57) allows us to disregard such corrections originating in d -subband. The second condition in Eq. (57) ensures that accounting for the inelastic scattering within d -subband reproduces the result of Section III for the relaxation rate $1/\tau_k$.

We write the Hamiltonian $H + \hat{V}_\Lambda$ acting in the reduced subspace r, l, d (see Fig 8) as

$$H + \hat{V}_\Lambda = H_d + H_{rl} + H_{d-rl}. \quad (58)$$

The first and second terms in the right-hand side here account for the states in “high-energy” subband d and the low-energy subbands r and l ,

$$H_d = P_d(H + \hat{V}_\Lambda)P_d, \quad H_{rl} = P_{rl}(H + \hat{V}_\Lambda)P_{rl},$$

where P_d and P_{rl} are projectors onto the corresponding states. The third term in Eq. (58) describes the interactions,

$$H_{d-rl} = P_d(H + \hat{V}_\Lambda)P_{rl} + P_{rl}(H + \hat{V}_\Lambda)P_d.$$

Using Hamiltonian Eq. (58), we evaluate the Green function of a particle in the subband d .

We start the evaluation of $G_k\left(\epsilon; \frac{\Lambda k^2}{mv}, \Lambda k\right)$ with accounting for the interaction terms in H_d . Evaluation of the self-energy follows the perturbative analysis of Section III. The only difference is that the second-order contribution to $\text{Im} \Sigma_k$, see Eq. (38), is absent provided that $|\epsilon - \xi_k^R| < \lambda k^2/mv$. Indeed, a finite $\text{Im} \Sigma_k^{(2)}$ requires excitation of a particle-hole pair in the l -subband. Such processes are absent in H_d but are included in H_{d-rl} discussed below. In addition, the second-order contribution to the real part of the self-energy, $\text{Re} \Sigma_k \sim \gamma_0^2(\epsilon - \xi_k^R) \ln(\Lambda/\lambda)$, can be also neglected as it is small compared with $|\epsilon - \xi_k^R|$. Unlike in the second order, the low-energy states (l and r subbands) do not play any special role in the fourth order calculation, see Section III. Hence, H_d alone is sufficient in order to reproduce the relaxation rate $1/2\tau_k$ (note that the term \hat{V}_Λ is important for this calculation). Thus, neglecting H_{d-rl} , we find for the retarded Green function

$$G_k^d\left(\epsilon; \frac{\Lambda k^2}{mv}, \Lambda k\right) = \frac{1}{\epsilon - \xi_k^R + i/2\tau_k}. \quad (59)$$

Next, we account for the effects of H_{d-rl} interaction on the Green function of a particle in the d -subband. For

this calculation \hat{V}_Λ is irrelevant. Moreover, the interaction between r and l subbands does not contribute to the Green function in the leading logarithmic approximation (this interaction leads merely to the higher-order corrections to the exponents). We thus neglect both these terms and write H_{rl} and H_{d-rl} as

$$H_{rl} = \sum_{\alpha=r,l} \sum_k \xi_k^\alpha \psi_k^{\alpha\dagger} \psi_k^\alpha \quad (60)$$

$$H_{d-rl} = (V_0 - V_k) \frac{1}{L} \sum_{|q| < \lambda k} \rho_q^d \rho_{-q}^r \quad (61)$$

$$+ (U_0 - U_{2p_F+k}) \frac{1}{L} \sum_{|q| < \lambda k^2/mv} \rho_q^d \rho_{-q}^l,$$

where the form of the interaction potentials $V_0 - V_k$ and $U_0 - U_{2p_F+k}$ originates in the reduction of the general interaction to the density-density form. Because of the strict limitation on the wavelengths of the density fluctuations, the subbands r and l do not contribute to $1/\tau_k$. Therefore the spectrum within these subbands can be linearized. Since both r and l subbands contain the Fermi level, the excitations within these subbands can be described using the conventional bosonization technique. Upon introducing the bosonic fields $\varphi_q^{r,l}$ such that $\rho_q^{r,l} = iq\varphi_q^{r,l}/2\pi$, we represent H_{rl} and H_{d-rl} in the form

$$H_{rl} = \frac{1}{4\pi L} \sum_{|q| < \lambda k} vq^2 |\varphi_q^r|^2 + \frac{1}{4\pi L} \sum_{|q| < \lambda k^2/mv} vq^2 |\varphi_q^l|^2 \quad (62)$$

$$H_{d-rl} = -i \frac{V_0 - V_k}{2\pi L} \sum_{|q| < \lambda k} q \rho_q^d \varphi_{-q}^r - i \frac{U_0 - U_{2p_F+k}}{2\pi L} \sum_{|q| < \lambda k^2/mv} q \rho_q^d \varphi_{-q}^l. \quad (63)$$

In the second order of perturbation theory the interactions in H_d can be neglected. The self-energy of d -particle is then given by the diagram shown in Fig. 9(a). Its evaluation reproduces the logarithmic divergence at $\epsilon \rightarrow \xi_k^R$, see Eq. (39).

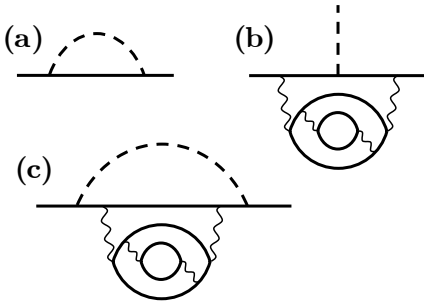


FIG. 9: (a) lowest-order logarithmic correction to the d -particle propagator (solid line); the dashed line stands for $r(l)$ bosons. (b) example of renormalization of the d -particle-boson vortex; wavy lines represent interaction within the d -subband. (c) one of the contributions to the decay rate of a d -particle.

To go beyond the lowest order, we need to take into account simultaneously both the interactions present in H_d as well as the interactions of d -particles with the bosons. Since we are interested in the limit $\epsilon - \xi_k^R \rightarrow 0$, it is sufficient to consider only the most divergent in this limit contributions.

Clearly, accounting for both types of interactions produces two kinds of contributions. First, interactions within the d -subband renormalize the particle-boson in-

teraction vertex. Vertex corrections such as that in Fig. 9(b) can be shown to be small (see Appendix A), and we neglect them hereinafter. Second, the interactions “dress” the bare d -particle Green function, see Fig. 9(c), replacing it by that given in Eq. (59). Obviously, the effect of the dressing is to cut the logarithmic divergencies off at $|\epsilon - \xi_k^R| \sim 1/\tau_k$.

The task of evaluating contributions such as that shown in Fig. 9(c) is greatly simplified by the fact that particle-boson interaction is associated with rather small ($\lesssim \lambda k$) transferred momentum. This allows us to linearize the d -particle spectrum about ξ_k^R ,

$$\xi_{k'}^d = \xi_{k+k'}^R \approx \xi_k^R + v_d k', \quad v_d = v + k/m.$$

It is convenient to write the d -particle Green function in the real space-time representation,

$$G_k \left(\epsilon; \frac{\Lambda k^2}{mv}, \Lambda k \right) = \int dx \int dt e^{i\epsilon t} G_k^d(\mathbf{x}), \quad \mathbf{x} \equiv (x, t).$$

In the absence of particle-boson interaction G_k^d satisfies the equation

$$\left(i \frac{\partial}{\partial t} + iv_d \frac{\partial}{\partial x} - \xi_k^R + \frac{i}{2\tau_k} \right) G_k^d(\mathbf{x}) = \delta(\mathbf{x}).$$

With vertex corrections neglected, the effect of the bosonic fields is merely to induce a slowly varying in space and time potential in which the d -particle moves. This fluctuating potential can be written as

$$\phi(x, t) = \frac{V_0 - V_k}{2\pi} \partial_x \varphi^r + \frac{U_0 - U_{2p_F+k}}{2\pi} \partial_x \varphi^l. \quad (64)$$

The retarded Green function of d -particle in the presence of the fluctuating potential $G_k^d(\mathbf{x}|\phi)$ satisfies the equation

$$\left(i \frac{\partial}{\partial t} + i v_d \frac{\partial}{\partial x} - \xi_k^R + \frac{i}{2\tau_k} + \phi(\mathbf{x}) \right) G_k^d(\mathbf{x}|\phi) = \delta(\mathbf{x}), \quad (65)$$

and $G_k^d(\mathbf{x})$ is obtained by averaging $G_k^d(\mathbf{x}|\phi)$ over the gaussian fluctuations of the field ϕ ,

$$G_k^d(\mathbf{x}) = \langle G_k^d(\mathbf{x}|\phi) \rangle_\phi.$$

Here $\langle \dots \rangle_\phi$ denotes the time-ordered averaging over the slowly varying field ϕ , see Eq. (64). Note that G_k^d in Eq. (65) describes propagation of a single d -particle in an empty band, hence the corresponding retarded Green function coincides with a time ordered one.

Carrying out the calculations, we find

$$G_k^d(\mathbf{x}|\phi) = -i\theta(t) \delta(x - v_d t) e^{-i\xi_k^R t - t/2\tau_k} e^{i[\theta(\mathbf{x}) - \theta(\mathbf{0})]} \quad (66)$$

with

$$\theta(\mathbf{x}) = \int \frac{d\omega}{2\pi} \sum_q \frac{i\phi(q, \omega)}{\omega - v_d q} e^{iqx - i\omega t}; \quad (67)$$

the summation over q here is restricted to $|q| < \lambda k$ for r - d interactions and to $|q| < \lambda k^2/mv$ for l - d interactions. Note that because θ enters Eq. (66) only in the combination $\theta(v_d t, t) - \theta(0, 0)$, the pole at $\omega = v_d q$ in Eq. (67) does not show up in Eq. (66).

With the dynamics of the bosonic fields described by a quadratic Hamiltonian Eq. (62), the averaging in Eqs. (66) and (67) is straightforward. It yields

$$G_k^d(\mathbf{x}) = -i\theta(t) \delta(x - v_d t) e^{-i\xi_k^R t - \frac{t}{2\tau_k} - K(\mathbf{x})}, \quad (68)$$

with

$$\begin{aligned} K(\mathbf{x}) &= \frac{1}{2} \langle (\theta(\mathbf{x}) - \theta(\mathbf{0}))^2 \rangle_\phi \\ &= \int \frac{d\omega}{2\pi} \sum_q \frac{\langle \phi(\mathbf{q})\phi(-\mathbf{q}) \rangle_\phi}{(\omega - v_d q)^2} (1 - \cos(qx - \omega t)). \end{aligned} \quad (69)$$

Here

$$\begin{aligned} \langle \phi(\mathbf{q})\phi(-\mathbf{q}) \rangle_\phi \\ = i(U_0 - U_{2p_F+k})^2 \Pi^l(\mathbf{q}) + i(V_0 - V_k)^2 \Pi^r(\mathbf{q}), \end{aligned} \quad (70)$$

and

$$\Pi^{r,l}(\mathbf{q}) = -i \langle \rho^{r,l} \rho^{r,l} \rangle_\phi = (q/2\pi) (\pm \omega - vq + i0 \operatorname{sgn} q)^{-1}$$

are density-density correlation functions for r and l bosons. Substitution of Eq. (70) into Eq. (69) and then into Eq. (68) yields

$$G_k^d(\mathbf{x}) = -i\theta(t) \delta(x - v_d t) e^{-i\xi_k^R t - t/2\tau_k} \exp \left\{ -\frac{\mu_{2p_F+k}^2}{4} \ln \left[1 + i \frac{\lambda k^2}{mv} (x + vt) \right] - \frac{\mu_k^2}{4} \ln [1 - i\lambda k(x - vt)] \right\}. \quad (71)$$

The Green function in the reduced band is given by the Fourier transform of this result (see Appendix B for the details of the calculation),

$$G_k \left(\epsilon; \frac{\Lambda k^2}{mv}, \Lambda k \right) = \frac{1}{\epsilon - \xi_k^R + i/2\tau_k} \left[\frac{\mu_{2p_F+k}^2}{4\gamma_k^2} \left(\frac{-\epsilon + \xi_k^R - i/2\tau_k}{\lambda k^2/m} \right)^{\gamma_k^2} + \frac{\mu_k^2}{4\gamma_k^2} \left(\frac{\epsilon - \xi_k^R + i/2\tau_k}{\lambda k^2/m} \right)^{\gamma_k^2} \right]. \quad (72)$$

Using now Eq. (54) and taking into account conditions Eq. (57), we finally arrive at the expression for the spectral function [the abbreviated versions of it were given in Eq. (7) and Eq. (11)]

$$A_k(\epsilon) = \frac{1}{4\pi} \left(\frac{\xi_k^R}{\epsilon_F} \right)^{\gamma_0^2} \left(\frac{k^2}{m} \right)^{\gamma_0^2 - \gamma_k^2} \operatorname{Im} \left\{ \frac{\mu_{2p_F+k}^2}{\gamma_k^2} \left(\frac{-1}{\epsilon - \xi_k^R + i/2\tau_k} \right)^{1 - \gamma_k^2} - \frac{\mu_k^2}{\gamma_k^2} \left(\frac{1}{\epsilon - \xi_k^R + i/2\tau_k} \right)^{1 - \gamma_k^2} \right\}. \quad (73)$$

The validity of the result (73) is restricted to the vicinity of the particle mass-shell, $|\epsilon - \xi_k^R| \lesssim \lambda k^2/2m$. It is clear however that well above the mass-shell, at $\epsilon - \xi_k^R \gg k^2/2m$, the dispersion nonlinearity has no effect and the spectral function crosses over to the conventional TL expression Eq. (4). On the other hand,

$\epsilon = \xi_k = \xi_k^R - k^2/m$ below the mass-shell represents the kinematic edge of the spectrum, see Section II. Evaluation of the spectral function in the immediate vicinity of the edge requires a special consideration, and is discussed in Section V below.

B. Vicinity of the hole mass-shell: $\epsilon \rightarrow \xi_k^R$, $k < 0$

The behavior of the spectral function near the hole mass-shell ($\epsilon \rightarrow \xi_k^R < 0$) is much simpler because the decay of a hole is prohibited by the energy and momentum conservation laws. The spectral function can be evaluated by following closely the route outlined in Section IV A apart from two important modifications: First, one needs to replace $1/\tau_k \rightarrow +i0$ in Eq. (65) and its solution. Second, unlike d -particle, d -hole has a velocity v_d which is smaller than v ; the difference is due to the positive curvature of the dispersion relation. This affects the analytical properties of Eq. (71). Indeed, at $x = v_d t$ the factors $x + vt$ and $x - vt$ have the same sign for $v_d < v$. This in turn results in $A_k(\epsilon) = 0$ at $\epsilon > \xi_k^R$, which agrees with the kinematic constraints on the hole part of the spectral function, see Section II. Below the mass-shell, at $0 < \xi_k^R - \epsilon \ll k^2/2m$, we find

$$G_k(\epsilon) = \left(\frac{|\xi_k^R|}{\epsilon_F^2} \right)^{\gamma_0} \frac{(k^2/m)^{\gamma_0 - \gamma_k^2}}{\epsilon - \xi_k^R + i0} \left(\frac{\epsilon - \xi_k^R + i0}{k^2/m} \right)^{\gamma_k^2}. \quad (74)$$

Imaginary part of this expression is given in Eq. (13).

V. EDGE SINGULARITIES

In the previous section we found that the spectral function diverges at the hole mass-shell, which coincides with the edge of the spectrum $\epsilon = \bar{\xi}_k$ at $k < 0$. Here we consider the behavior of the spectral function in the vicinity of the remaining kinematic boundaries. As discussed in Section II, in all cases the spectral function exhibits a power-law suppression at the edge. The suppression originates in the phase space constraints which lead to vanishing of the spectral function linearly with the distance to the edge. Interactions modify the exponent via a mechanism analogous to the X-ray edge singularity in metals²³: the transition amplitudes in Eqs. (14) and (21) acquire a power-law dependence on the distance to the edge. In this Section we develop a technique to account for this dependence.

The edge of the spectrum corresponds to final states of the transition in which all of the momentum and energy are carried by a single hole, see Section II. At energies close to, but not precisely at, the kinematic edge, the final states may contain, in addition to this ‘‘deep hole’’, an arbitrary number of low-energy particle-hole pairs near the two Fermi points.

When the distance in energy to the corresponding edge is small compared to k^2/m , the hole can be treated as distinguishable from the rest of the particles in the system^{8,10}. Formally, this amounts to projecting out all states except those in the narrow stripes of momenta r, l near the Fermi points, and a strip d deep below the Fermi level. (Note the difference between the narrow d -subband defined in this Section and the wide one in Section IV). The d -subband hosts a single hole, and the interaction

of this hole with the rest of the system results in the excitation of the particle-hole pairs in the subbands r and l .

We consider first the behavior of the spectral function near the hole edge $\epsilon \approx \bar{\xi}_k$ at $k > 0$, and then proceed with the consideration of the particle edge $\epsilon \approx \underline{\xi}_k$.

A. $\epsilon \rightarrow \bar{\xi}_k$, $k > 0$

In this case the deep hole in the final state of the transition is located at momentum close to k (relative to $-p_F$) on the left-moving branch of the spectrum, see Fig. 10. In order to describe the final-state interaction, we project the Hamiltonian (34) onto narrow strips of momenta shown in Fig. 10, $H_{\text{eff}} = \mathcal{P}H\mathcal{P}$, where \mathcal{P} projects onto states within r, l , and d -subbands, while the remaining states are regarded as either occupied or empty. In order to extract the dependence of the spectral function on the distance to the edge with the leading logarithmic accuracy, it is sufficient to carry out the projection to zero order in interactions for the Hamiltonian and to the lowest nonvanishing (first) order for the observable. The omitted higher order contributions would contribute beyond the leading logarithmic accuracy.

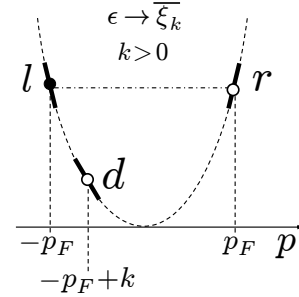


FIG. 10: Solid lines indicate the states included in the effective Hamiltonian (76)-(80). The d -subband hosts a single hole. The interaction of the hole with r and l -subbands leads to the excitation of low-energy particle-hole pairs. Production of multiple particle-hole pairs results in a power-law dependence of the spectral function in a close analogy with X-ray edge singularity in metals.

We introduce slowly varying in space fields

$$\psi^{r,l}(x) = \sum_{|k| < k_0} \frac{e^{ikx}}{\sqrt{L}} \psi_k^{R,L}, \quad \psi^d(x) = \sum_{|k'| < k_0} \frac{e^{ik'x}}{\sqrt{L}} \psi_{k+k'}^L \quad (75)$$

where $k_0 \ll k$ is the high-momentum cutoff, and write the effective Hamiltonian in the coordinate representation as

$$H_{\text{eff}} = H_{rl} + H_d + H_{\text{int}}. \quad (76)$$

Here

$$H_{rl} = \int dx [\psi^{r\dagger}(-iv\partial_x)\psi^r + \psi^{l\dagger}(iv\partial_x)\psi^l] \quad (77)$$

and

$$H_d = \int dx \psi^{d\dagger} (\bar{\xi}_k + iv_d \partial_x) \psi^d \quad (78)$$

describe r, l , and d subbands, respectively. In writing Eqs. (77) and (78) we linearized the spectrum within the respective subbands, so that

$$\xi_{k+k'}^L = \bar{\xi}_k - v_d k', \quad v_d = v - k/m. \quad (79)$$

The third term in the right-hand side of Eq. (76) describes the interaction between the subbands,

$$\begin{aligned} H_{\text{int}} = & - \int dx \bar{\rho}^d [(V_0 - V_k) \rho^l + (V_0 - V_{2p_F - k}) \rho^r] \\ & + (V_0 - V_{2p_F}) \int dx \rho^r(x) \rho^l(x), \end{aligned} \quad (80)$$

where $\rho^{r,l}(x) = \psi^{r,l\dagger}(x) \psi^{r,l}(x)$ are particle densities in r, l -subbands, and $\bar{\rho}^d(x) = \psi^d(x) \psi^{d\dagger}(x)$ is density of holes in d -subband. In writing Eq. (80) we have set $V_q = U_q$.

Our goal is to evaluate the hole contribution to the spectral function

$$A_k(\epsilon) = \text{Re} \frac{1}{\pi} \int_{-\infty}^0 dt e^{-i\epsilon t} \langle \psi_k^{R\dagger}(t) \psi_k^R(0) \rangle. \quad (81)$$

The projection should now be applied to the operator ψ_k^R in Eq. (81). In this case, however, the lowest order is insufficient, as the state with momentum k on the right-moving branch of the spectrum lies outside the subbands r, l, d of the effective Hamiltonian. Instead, the relevant contribution is generated in the first order in the interaction strength.

The higher-order contributions can be found with the help of a unitary (Schrieffer-Wolff) transformation that decouples states within the subbands r, l , and d from the rest of the system. Consider the following term in the original Hamiltonian (34),

$$\begin{aligned} \delta H = & (V_k - V_{2p_F}) \frac{1}{L} \sum_{|k_i| < k_0} \delta_{k_1+k_2, k_3} \\ & \times (1 - \mathcal{P}) \psi_k^{R\dagger} \psi_{k_1}^R \psi_{k_2}^{L\dagger} \psi_{k+k_3}^L \mathcal{P} + \text{H.c.} \end{aligned} \quad (82)$$

Schrieffer-Wolff transformation $H \rightarrow e^{i\hat{S}} H e^{-i\hat{S}}$ eliminates the off-diagonal contributions such as Eq. (82). To the lowest (first) order in the interaction strength, the generator of such transformation reads

$$\begin{aligned} \hat{S} = & \frac{V_k - V_{2p_F}}{iL(\xi_k^R - \xi_k^L)} \sum_{|k_i| < k_0} \delta_{k_1+k_2, k_3} \\ & \times (1 - \mathcal{P}) \psi_k^{R\dagger} \psi_{k_1}^R \psi_{k_2}^{L\dagger} \psi_{k+k_3}^L \mathcal{P} + \text{H.c.}, \end{aligned}$$

so that $[i\hat{S}, H_0] = -\delta H$, where H_0 is the noninteracting part of Eq. (34).

As far as the effective Hamiltonian (76) is concerned, the transformation leads merely to the correction to H_{int} ,

$$\delta H_{\text{int}} = \frac{1}{2} [i\hat{S}, \delta H],$$

which amounts to negligible second-order corrections to the coupling constants in Eq. (80).

The same Schrieffer-Wolff transformation applied to the operator ψ_k^R yields

$$\begin{aligned} \psi_k^R & \rightarrow [i\hat{S}, \psi_k^R] \\ & = -\frac{V_k - V_{2p_F}}{\xi_k^R - \xi_k^L} \frac{1}{L} \sum_{|k_i| < k_0} \psi_{k_1}^{L\dagger} \psi_{k_2}^R \psi_{k+k_3}^L \delta_{k_1, k_2+k_3}. \end{aligned} \quad (83)$$

This contribution, as well as those generated in higher orders, conserves separately the numbers of right- and left-movers. With this constraint, the first-order contribution (83) is a product of the least possible number of operators acting in the subbands r, l, d , hence, it is the most relevant one as far as the behavior of the spectral function near the edge is concerned.

Using now Eqs. (75), (81), and (83), we find

$$A_k(\epsilon) \propto \text{Re} \int dx \int_{-\infty}^0 dt e^{-i\epsilon t} \langle \Psi^\dagger(x, t) \Psi(0, 0) \rangle \quad (84)$$

with

$$\Psi(x) = \psi^{l\dagger}(x) \psi^r(x) \psi^d(x). \quad (85)$$

To proceed further, we bosonize fermions in r and l -subbands according to

$$\psi^{r,l} = \sqrt{k_0} e^{\pm i\varphi^{r,l}}, \quad [\varphi^{r,l}(x), \varphi^{r,l}(y)] = \pm i\pi \text{sgn}(x-y), \quad (86)$$

where the upper/lower sign corresponds to r/l , and k_0 is high-momentum cutoff for bosonic modes,

$$\langle \varphi^{r,l}(x) \varphi^{r,l}(0) - [\varphi^{r,l}(0)]^2 \rangle = -\ln(1 \mp 2\pi i k_0 x).$$

In the bosonic representation Eqs. (77) and (80) read

$$H_{rl} = \frac{v}{4\pi} \sum_{\alpha=r,l} \int dx (\partial_x \varphi^\alpha)^2 \quad (87)$$

$$\begin{aligned} H_{\text{int}} = & - \int \frac{dx}{2\pi} \bar{\rho}^d [(V_0 - V_k) \partial_x \varphi^l + (V_0 - V_{2p_F - k}) \partial_x \varphi^r] \\ & + (V_0 - V_{2p_F}) \int \frac{dx}{(2\pi)^2} (\partial_x \varphi^r) (\partial_x \varphi^l), \end{aligned} \quad (88)$$

and Eq. (85) becomes

$$\Psi(x) = k_0 e^{i[\varphi^r(x) + \varphi^l(x)]} \psi^d(x). \quad (89)$$

The correlation function (84) with Ψ given by Eq. (89) and with the dynamics governed by the effective Hamiltonian (78), (87), and (88) can be evaluated exactly. This

can be done by following the steps outlined in Section IV. Equivalently, one can diagonalize the effective Hamiltonian by an appropriate unitary transformation^{8,10}. The generator of such transformation reads

$$\widehat{W} = \frac{1}{2} \int dx \bar{\rho}_d(x) [\mu_{2p_F-k} \varphi^r(x) - \mu_k \varphi^l(x)] \quad (90)$$

$$+ \frac{\mu_{2p_F}}{8\pi} \int dx [\varphi^r \partial_x \varphi^l - \varphi^l \partial_x \varphi^r]$$

with μ_k introduced in Eq. (9) above. In writing Eq. (90) we omitted all but the first-order in interactions contributions (recall that second and higher order corrections have been neglected in the derivation of the effective Hamiltonian). The transformation decouples the subbands from each other to linear order in interactions,

$$e^{i\widehat{W}} H_{\text{eff}} e^{-i\widehat{W}} = H_{rl} + H_d, \quad (91)$$

and also modifies the operator Ψ , see Eq. (89),

$$e^{i\widehat{W}} \Psi e^{-i\widehat{W}} \propto \psi^d e^{i[1+\frac{1}{2}(\mu_{2p_F-k}-\mu_{2p_F})] \varphi^r} e^{i[1-\frac{1}{2}(\mu_k+\mu_{2p_F})] \varphi^l} \quad (92)$$

Since the transformed Hamiltonian (91) is quadratic, evaluation of the correlation function Eq. (84) is straightforward. Keeping only linear in μ_p terms in the exponents, we find

$$\langle \Psi^\dagger(x, t) \Psi(0, 0) \rangle \propto \delta(x + v_d t) e^{i\bar{\xi}_k t} \quad (93)$$

$$\times k_0 [1 + 2\pi i k_0 (v t - x)]^{-1 - \mu_{2p_F-k} + \mu_{2p_F}}$$

$$\times k_0 [1 + 2\pi i k_0 (v t + x)]^{-1 + \mu_k + \mu_{2p_F}}.$$

Substitution of Eq. (93) into Eq. (84) then yields the spectral function near the edge,

$$A_k(\epsilon) \propto (\bar{\xi}_k - \epsilon)^{1 - \mu_k + \mu_{2p_F-k} - 2\mu_{2p_F}} \theta(\bar{\xi}_k - \epsilon), \quad (94)$$

see Eq. (28). This result is valid when ϵ is close to the edge, $\bar{\xi}_k - \epsilon \ll k^2/m$, and for $0 < k < 2p_F$ (note that for $k > p_F$ the above derivation should be modified as in this case d -subband in the corresponding effective Hamiltonian belongs to the right-moving branch of the spectrum).

The interaction-induced corrections to +1 in the exponent in Eq. (94) (which comes from the phase-space constraints) allow for a simple interpretation based on the analogy with X-ray edge singularity²³ in metals: $-\mu_k$ originates in the attractive interaction of the deep hole on the left-moving branch of the spectrum with a soft left-moving particle; μ_{2p_F-k} is due to the repulsion between the deep hole and a soft right-moving hole; finally, $-2\mu_{2p_F}$ is due to the attraction between a soft left-moving particle and a soft right-moving hole (note that both particles are soft, hence the factor of 2).

For small k , the exponent in Eq. (94) simplifies to

$$1 - \mu_k + \mu_{2p_F-k} - 2\mu_{2p_F} \rightarrow 1 - \mu_k - \mu_{2p_F} \rightarrow 1 - 2\gamma_0,$$

where we used $\mu_{2p_F} = 2\gamma_0$ and the fact that for a generic interaction $\mu_k \rightarrow 0$ when $k \rightarrow 0$.

B. $\epsilon \rightarrow \underline{\xi}_k$, $k < 0$

The consideration in this case is very similar to that in Section VA. The effective Hamiltonian accounting for the final-state interaction again consists of subbands r and l near the two Fermi points, and d -subband (now centered at momentum $-k > 0$) deep below the Fermi level on the left branch of the spectrum, see Fig. 11. The projection, carried out to the lowest order in interactions, yields Eqs. (76)-(80) with the replacement $\bar{\xi}_k \rightarrow -\underline{\xi}_k$ and $v_d \rightarrow v + k/m$ in Eq. (78), and $k \rightarrow -k$ in Eq. (80).

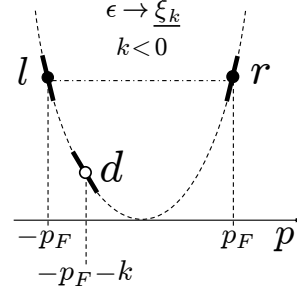


FIG. 11: Solid lines indicate the subbands r, l , and d in the effective Hamiltonian for the evaluation of the particle contribution to the spectral function at $\epsilon \rightarrow \underline{\xi}_k$, $k < 0$.

The particle contribution to the spectral function is given by

$$A_k(\epsilon) = \text{Re} \frac{1}{\pi} \int_0^\infty dt e^{i\epsilon t} \langle \psi_k^R(t) \psi_k^{R\dagger}(0) \rangle. \quad (95)$$

Similar to above, application of the Schrieffer-Wolff transformation to the operator $\psi_k^{R\dagger}$ yields the relevant contribution in the first order in the interaction strength,

$$\psi_k^{R\dagger} \propto \frac{V_k - V_{2p_F+k}}{\xi_k^R + \xi_{-k}^L} \frac{1}{L} \sum_{|k_i| < k_0} \psi_{k_1}^{R\dagger} \psi_{k_2}^L \psi_{-k+k_3}^L \delta_{k_1+k_2, k_3}. \quad (96)$$

When written in the coordinate representation, Eqs. (95) and (96) give

$$A_k(\epsilon) \propto \text{Re} \int dx \int_0^\infty dt e^{i\epsilon t} \langle \Psi(x, t) \Psi^\dagger(0, 0) \rangle \quad (97)$$

with

$$\Psi^\dagger(x) = \psi^{r\dagger}(x) \psi^{l\dagger}(x) \psi^d(x). \quad (98)$$

The spectral function (97) is evaluated by bosonizing the Hamiltonian and diagonalizing it by a unitary transformation, just as it is done in Section VA. This procedure yields

$$A_k(\epsilon) \propto (\epsilon - \underline{\xi}_k)^{1 - \mu_k - \mu_{2p_F+k} + 2\mu_{2p_F}} \theta(\epsilon - \underline{\xi}_k). \quad (99)$$

This result is valid at $\epsilon - \underline{\xi}_k \ll k^2/m$, and for all k in the range $-2p_F < k < 0$. Note that μ_{2p_F} and μ_{2p_F+k} enter

the exponent in Eq. (99) with opposite signs compared to those in Eq. (94). This is because the interaction of the deep hole with a particle on the r -branch is *attractive*, whereas the corresponding correction to the exponent in Eq. (94) originates in the *repulsion* between the deep hole and another hole in r -subband.

As expected, the exponent in Eq. (99) is invariant upon the momentum inversion $k \leftrightarrow 2p_F + k$. At very small $|k|$, the exponent in Eq. (99) simplifies to

$$1 - \mu_k - \mu_{2p_F+k} + 2\mu_{2p_F} \rightarrow 1 + \mu_{2p_F} = 1 + 2\gamma_0.$$

C. $\epsilon \rightarrow \underline{\xi}_k$, $k > 0$

In this limit the final state of the transition involves creation of a hole with the momentum $-k$ on the right-moving branch of the spectrum, see Fig. 12 and discussion in Section II. In order to evaluate the spectral function in the leading logarithmic approximation, it is sufficient to consider the effective Hamiltonian consisting of d -subband hosting the hole, and r -subband to allow for the creation of low-energy particle-hole pairs near the right Fermi point, see Fig. 12. (Inclusion of left-movers would merely add a second-order in interaction correction to the exponent.) Carrying out the projection and linearizing the spectrum within the subbands, we find

$$H_{\text{eff}} = H_r + H_d + H_{\text{int}} \quad (100)$$

with

$$H_r = \int dx \psi^{r\dagger} (-iv\partial_x) \psi^r, \quad (101)$$

$$H_d = \int dx \psi^{d\dagger} (-\underline{\xi}_k - iv_d \partial_x) \psi^d \quad (102)$$

(here $v_d = v - k/m$), and

$$H_{\text{int}} = -(V_0 - V_k) \int dx \bar{\rho}^d(x) \rho^r(x). \quad (103)$$

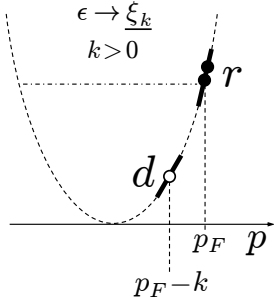


FIG. 12: States included in the effective Hamiltonian (100)-(103) for the evaluation of the spectral function at $\epsilon \rightarrow \underline{\xi}_k$, $k > 0$.

After bosonizing Eqs. (101) and (103), the effective Hamiltonian can be diagonalized by a unitary transfor-

mation with generator

$$\widehat{W} = -\frac{\mu_k}{2} \int dx \bar{\rho}^d(x) \varphi^r(x). \quad (104)$$

The transformation yields, to first order in the interaction strength,

$$e^{i\widehat{W}} H_{\text{eff}} e^{-i\widehat{W}} = H_r + H_d, \quad (105)$$

where $H_r = (v/4\pi) \int dx (\partial_x \varphi^r)^2$ and H_d is given by Eq. (102).

Since the right-moving state with momentum $k \gg k_0$ lies outside the domain of the effective Hamiltonian (100), application of the lowest-order projection to the operator $\psi_k^{R\dagger}$, see Eq. (95), is insufficient. Similar to above, the relevant contribution emerges in the first order in the interaction strength and reads

$$\psi_k^{R\dagger} \propto \frac{1}{L} \sum_{|k_i| < k_0} \frac{V_{k-k_1} - V_{k-k_2}}{\xi_k^R + \xi_{-k}^R} \psi_{k_1}^{R\dagger} \psi_{k_2}^{R\dagger} \psi_{-k+k_3}^R \delta_{k_1+k_2, k_3}. \quad (106)$$

Since $k_0 \ll k$, we can expand here

$$V_{k-k_1} - V_{k-k_2} \approx (k_2 - k_1) \frac{dV_k}{dk}.$$

Passing over to the coordinate representation, we find that the spectral function is given by Eq. (97) with

$$\Psi^\dagger(x) = \psi^{r\dagger}(x) (-i\partial_x) \psi^{r\dagger}(x) \psi^d(x). \quad (107)$$

Bosonizing Eq. (107) according to Eq. (86) and taking proper care of the point splitting (see Appendix C for the details), we find

$$\Psi^\dagger(x) = 2\pi k_0^2 e^{-2i\varphi^r(x)} \psi^d(x). \quad (108)$$

The unitary transformation (104)-(105) that diagonalizes the effective Hamiltonian also modifies the operator Ψ^\dagger :

$$e^{i\widehat{W}} \Psi^\dagger(x) e^{-i\widehat{W}} \propto e^{-i(2-\mu_k/2)\varphi^r(x)} \psi^d(x). \quad (109)$$

With the dynamics governed by the quadratic Hamiltonian (105), it is straightforward to calculate

$$\langle \Psi(x, t) \Psi^\dagger(0, 0) \rangle \propto \delta(x - v_d t) e^{-i\underline{\xi}_k t} \times k_0^4 [1 + 2\pi i k_0 (v t - x)]^{-4+2\mu_k}. \quad (110)$$

Substitution of Eq. (110) into Eq. (97) then yields

$$A_k(\epsilon) \propto (\epsilon - \underline{\xi}_k)^{3-2\mu_k} \theta(\epsilon - \underline{\xi}_k) \quad (111)$$

for the spectral function at $\epsilon - \underline{\xi}_k \ll k^2/m$. The fact that the interaction-induced correction to the exponent is $-2\mu_k$ is due to the presence of two soft particles interacting with the deep hole, contributing $-\mu_k$ each.

VI. CALOGERO-SUTHERLAND MODEL

In this section we consider a solvable model of interacting 1D fermions, the Calogero-Sutherland (CS) model. The corresponding Hamiltonian in the first-quantized form reads²⁸

$$H = - \sum_i \frac{1}{2m} \frac{\partial^2}{\partial x_i^2} + \sum_{i < j} V(x_i - x_j), \quad (112)$$

where $V(x)$ is a periodic version of the inverse-square interaction potential,

$$V(x) = \frac{\lambda(\lambda - 1)/m}{(L/\pi)^2 \sin^2(\pi x/L)}. \quad (113)$$

Correlation functions of the CS model exhibit rather unusual behavior. For example, the dynamic structure factor $S(q, \omega)$ differs from zero in a finite interval of frequencies^{6,10,29,30}, just as it is for free fermions. On the contrary, for a generic interaction the structure factor has a high-frequency “tail” $S \propto q^4/\omega^2$, which emerges already in the second order of the perturbation theory in the interaction strength^{6,8}. However, close examination of the corresponding perturbative formula for the structure factor (see Eq. (18) of Ref. [6]) indeed shows that it yields zero for $V_k \propto |k|$.

Similarly, substitution of $U_k = V_k \propto |k|$ into Eqs. (40)-(43) yields $1/2\tau_k = -\text{Im} \Sigma_k^{(4)}(\xi_k) \equiv 0$. Just as it is the case with the absence of the high-frequency tail in $S(q, \omega)$, the apparent vanishing of the relaxation rate in perturbation theory suggests that $1/\tau_k = 0$ is the exact relation for the CS model. Indeed, this agrees with the exact results for the Green function²⁹ obtained for specific values of λ .

Vanishing of $1/\tau_k$ for particles is a peculiar property of the CS model related to its integrability²¹. Therefore, in the context of this work, we concentrate on the *hole* contribution to the spectral function; we believe that the CS model results for the hole ($\epsilon < 0$) region of the spectrum are generic.

Single-particle correlation functions for the CS model have been studied extensively^{29,30} in the context of the exclusion statistics³¹. Such interpretation is possible because the inverse-square potential is impenetrable. Requiring the many-body wave function to obey a certain symmetry with respect to the permutations of the particles' coordinates amounts to merely choosing a rule according to which the wave function is assigned an overall phase. For CS model, the phase depends on the ordering of particles, but not on their coordinates. Operators which do not permute particles (e.g., the local density operator) do not affect the phase factor. Accordingly, the statistics of bare particles is immaterial as far as the evaluation of, say, the dynamic structure factor $S(q, \omega)$ is concerned¹⁰.

However, the situation with single-particle correlation functions is more subtle. The anyon creation and annihilation operators constructed and studied in Ref. [29,30]

describe fermions only for odd integer values of λ . Rather than attempting to derive fermionic Green function for general values of λ , below we will use the results of Refs. [30] to evaluate $A_k(\epsilon)$ for $\epsilon < 0$ and $\lambda = \text{odd integer}$, and then employ an analytical continuation to extend the result to arbitrary values of λ .

The excitations of CS model can be described in terms of quasiparticles and quasiholes. Quasiholes are characterized by fractional inertial mass $\bar{m} = m/\lambda$ and velocities v_i in the range $|v_i| < v = p_F/\bar{m}$, where $p_F = \pi n$ is the Fermi momentum (n is particle concentration). On the contrary, quasiparticles have velocities $|v_i| > v$ and their mass coincides with the bare mass m that enters Eq. (112).

Consider now a state obtained by a removal of a single particle (with mass m) from the ground state $|0\rangle$. For integer λ , this change of mass can be accommodated by creation of exactly λ quasiholes. It turns out that this simplest possibility is, in fact, exhaustive³⁰.

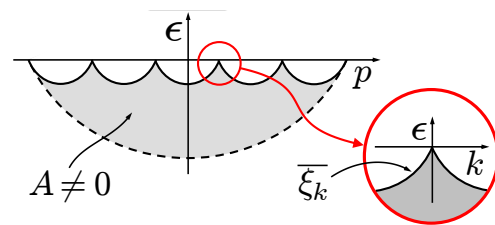


FIG. 13: Support of the spectral function in $(p, \epsilon < 0)$ half-plane. The upper boundary of the region where $A \neq 0$ comprises of λ identical parabolic segments ($\lambda = 5$ in the figure). We concentrate on the low-energy sector $k = p - p_F \rightarrow 0$ (see the inset).

The region of support of $A_p(\epsilon)$ in (p, ϵ) -plane can now be deduced from the energy and momentum conservation. Indeed, using the well-known expressions²⁸ for the energy and momentum of a state with λ quasiholes with velocities v_i , one can write

$$\epsilon + \sum_{i=1}^{\lambda} \frac{\bar{m}}{2} (v^2 - v_i^2) = 0, \quad p - \sum_{i=1}^{\lambda} \bar{m} v_i = 0. \quad (114)$$

For odd integer λ , these equations have a solution for $\{v_i\}$ provided that ϵ and p lie within the shaded region in Fig. 13. The upper boundary of this region, the solid line $\epsilon = \bar{\xi}_p$, comprises of λ identical parabolic segments,

$$\bar{\xi}_p = \frac{1}{2\bar{m}} [(p - 2lp_F)^2 - p_F^2], \quad |p - 2lp_F| < p_F \quad (115)$$

with integer l , $|l| \leq (\lambda - 1)/2$. The support of $A_p(\epsilon)$ is also bounded from below by the dashed line $\epsilon = p^2/2m - \epsilon_F$ with $\epsilon_F = mv^2/2$; this boundary would be absent for generic values of λ .

We concentrate here on the low-energy sector with $p \approx p_F$, $|\epsilon| \ll \epsilon_F$ (see Fig. 13) and “shift” the momentum according to $k = p - p_F$. The dependence of $A_k(\epsilon)$ on ϵ

has a threshold,

$$A_k(\epsilon) \propto \theta(\overline{\xi_k} - \epsilon), \quad \overline{\xi_k} = -v|k| + k^2/2\bar{m}, \quad (116)$$

and our goal here is to find the behavior of A at a fixed k when ϵ approaches the threshold. This can be done by writing the spectral function in the form of a multiple integral,

$$A_k(\epsilon) \propto m \int_{-v}^v \prod_{i=1}^{\lambda} dv_i F(\{v_i\}) \quad (117)$$

$$\times \delta[k + p_F - \bar{m}\sum v_i] \delta[\epsilon + (\bar{m}/2)\sum(v^2 - v_i^2)].$$

The δ -functions here reflect the conservation of momentum and energy, see Eq. (114), and the form-factor $F \propto |\langle \{v_i\} | \psi_k | 0 \rangle|^2$ was found in Ref. [30],

$$F(\{v_i\}) = \prod_{i_1 < i_2} |v_{i_1} - v_{i_2}|^{2/\lambda} \prod_i (v^2 - v_i^2)^{-\frac{\lambda-1}{\lambda}}. \quad (118)$$

Eq. (117) is nothing but the Lehmann representation of the spectral function, with the final state of the transition $|\{v_i\}\rangle$ parametrized by the velocities of λ quasiholes.

For $|k| \ll p_F$ and $\overline{\xi_k} - \epsilon \ll \epsilon_F$, the final states $\{v_i\}$ contributing to A have $n_\lambda = (\lambda - 1)/2$ quasiholes with velocities $v_i \approx -v$ and $n_\lambda + 1$ quasiholes with velocities $v_i \approx +v$. It is therefore convenient to introduce new variables

$$x_i = \frac{v - v_i}{v}, \quad y_i = \frac{v + v_i}{v}.$$

After expansion of the form-factor to the lowest nonvanishing order in $x_i, y_i \ll 1$, Eq. (117) takes the form

$$A_k(\epsilon) \propto \frac{1}{\epsilon_F} \prod_{i,j} \int_0^\infty dx_i \int_0^\infty dy_j f_{n_\lambda+1}(\{x_i\}) f_{n_\lambda}(\{y_j\})$$

$$\times \delta\left[\frac{\epsilon + vk}{2\bar{m}v^2} + X_1 - \frac{1}{4}(X_2 + Y_2)\right] \quad (119)$$

$$\times \delta\left[\frac{\epsilon - vk}{2\bar{m}v^2} + Y_1 - \frac{1}{4}(X_2 + Y_2)\right].$$

Here

$$X_n = \sum_{i=1}^{n_\lambda+1} x_i^n, \quad Y_n = \sum_{i=1}^{n_\lambda} y_i^n,$$

and $f_N(\{z_i\})$ is a function of N arguments z_1, \dots, z_N given by

$$f_N(\{z_i\}) = \prod_{i_1 < i_2} |z_{i_1} - z_{i_2}|^{2/\lambda} \prod_i z_i^{-\frac{\lambda-1}{\lambda}}; \quad (120)$$

this is a homogeneous function of degree

$$c_N = \frac{1}{4\lambda} \left\{ [2(N - n_\lambda) - 1]^2 - \lambda^2 \right\}.$$

As it is easy to check,

$$X_2 \sim X_1^2 \ll X_1 \ll 1, \quad Y_2 \sim Y_1^2 \ll Y_1 \ll 1.$$

Moreover, when ϵ is relatively far from the threshold, at $\overline{\xi_k} - \epsilon \gg k^2/2\bar{m}$, X_1 and Y_1 are of the same order, $X_1 \sim Y_1$. In this limit X_2 and Y_2 in the arguments of the δ -functions in Eq. (119) can be safely neglected, after which the integration reduces to a power counting which yields

$$A_k(\epsilon) \propto |\epsilon + vk|^{\gamma_0^2} |\epsilon - vk|^{\gamma_0^2-1}, \quad \overline{\xi_k} - \epsilon \gg k^2/\bar{m} \quad (121)$$

with

$$\gamma_0^2 = \frac{(\lambda - 1)^2}{4\lambda}. \quad (122)$$

Eqs. (121) and (122) reproduce the standard Luttinger liquid result. At $|vk - \epsilon| \ll v|k|$ Eq. (121) agrees with Eq. (4) above. Since the exponent γ_0 is an analytical function of λ , Eq. (122) is valid for all λ rather than for integer values only. Indeed, in the weak interaction limit $|\lambda - 1| \ll 1$, Eq. (5) yields $\gamma_0 \approx (\lambda - 1)/2$, in agreement with the corresponding limit of Eq. (122).

The behavior of the spectral function in the immediate vicinity of the threshold, at $\overline{\xi_k} - \epsilon \lesssim k^2/\bar{m}$, requires more delicate consideration. Indeed, in this limit the velocity of one of the quasiholes approaches

$$v_0(k) = -v \operatorname{sgn}(k) + k/\bar{m}, \quad (123)$$

while all other quasiholes have velocities $v_i \rightarrow \pm v$. In other words, close to the threshold, almost all of the momentum and energy are carried by a single quasihole,

$$\overline{\xi_k} = -\frac{\bar{m}}{2} [v^2 - v_0^2(k)].$$

In order to evaluate the integral in Eq. (119), we note that for $\overline{\xi_k} - \epsilon \ll k^2/\bar{m}$ and $\alpha = |k/p_F| \ll 1$ the conservation laws [i.e., the δ -functions in Eq. (119)] imply that for $k < 0$

$$X_1 \approx \alpha, \quad X_2 \sim Y_1 \sim \alpha^2.$$

Actually, for $k < 0$ it is just one of x_i , say, $x_{n_\lambda+1}$, which is close to α , while for $i = 1, \dots, n_\lambda$ one has $x_i \sim \alpha^2$. It is therefore convenient to write

$$x_{n_\lambda+1} = \alpha + x_0, \quad x_0 \sim \alpha^2,$$

and introduce $\tilde{X}_1 = X_1 - \alpha = \sum_{i=0}^{n_\lambda} x_i \sim \alpha^2$. In the leading (second) order in α the δ -functions in Eq. (119) can be approximated by

$$\delta\left(\frac{\overline{\xi_k} - \epsilon}{2\bar{m}v^2} - \tilde{X}_1\right) \delta\left(\frac{\overline{\xi_k} - \epsilon}{2\bar{m}v^2} - Y_1\right)$$

[note that $0 < (\overline{\xi_k} - \epsilon)/\bar{m}v^2 \lesssim \alpha^2$]. At the same time, $x_{n_\lambda+1}$ in the form-factor should be replaced by α . With

these approximations, the remaining integrations are easily carried out resulting in

$$A_{k<0}(\epsilon) \propto (\overline{\xi}_k - \epsilon)^{2\gamma_0^2 - 1}, \quad 0 < \overline{\xi}_k - \epsilon \lesssim k^2/\bar{m} \quad (124)$$

The fractional part of the exponent here is twice that in the Luttinger liquid limit, see Eq. (121). This is in agreement with the leading logarithmic approximation result $A_{k<0}(\epsilon) \propto (\overline{\xi}_k - \epsilon)^{\gamma_k^2 - 1}$, see Eq. (13). Indeed, substitution of $V_k = -\lambda(\lambda - 1)\pi|k|/m$ into Eq. (9) gives $\mu_k = \mu_0 \approx \lambda - 1$, independently of k (this agrees with the exact value¹⁰ of the exponent that governs the divergence of the structure factor, $\mu_0 = 1 - 1/\lambda$). Eq. (8) then yields $\gamma_k^2 = \mu_0^2/2 \approx 2\gamma_0^2$. Note also that the position of the spectral edge $\overline{\xi}_k$, see Eq. (116), in the limit $\lambda \rightarrow 1$ agrees with Eq. (24).

Evaluation of $A_k(\epsilon)$ for $k > 0$ proceeds similarly and yields

$$A_{k>0}(\epsilon) \propto (\overline{\xi}_k - \epsilon)^{\gamma_0^2 + \gamma_1^2}, \quad 0 < \overline{\xi}_k - \epsilon \lesssim k^2/\bar{m} \quad (125)$$

with γ_1 given by

$$\gamma_1^2 = \frac{(\lambda - 3)^2}{4\lambda}. \quad (126)$$

For a weak interaction $\gamma_0^2 + \gamma_1^2 \approx 1 - 2\mu_0$, in agreement with Eqs. (28) and (94). Note that the exact exponent in Eq. (125) is positive for any strength of interactions.

We have thus demonstrated that, at least in the hole region of the spectrum $\epsilon < 0$, the behavior expected for a generic 1D system with a nonlinear dispersion is consistent with the exact results obtained for the Calogero-Sutherland model. It would be interesting to find a solvable model for which our conclusions for the particle region of the spectrum can be similarly tested.

VII. CONCLUSIONS

The total number of particles and the total momentum are good quantum numbers for an isolated homogeneous fermionic system, regardless of its dimensionality and the interaction strength. In higher dimensions ($D > 1$) and for moderately strong interactions, an excited state of the system with one extra particle and with momentum p is rather similar to the corresponding state of a free Fermi gas. The similarity is encoded in the energy and momentum dependence of the spectral function $A_p(\epsilon) = -(1/\pi) \text{Im} G_p(\epsilon)$. The spectral function satisfies the exact sum rule,

$$\int d\epsilon A_p(\epsilon) = 1. \quad (127)$$

In a Fermi liquid ($D > 1$), the sum rule is almost completely exhausted by the Lorentzian Eq. (1). The corresponding peak is centered at the quasiparticle energy ξ_p and has the width $1/2\tau_p$ which decreases with the increase of the Fermi energy, see Eq. (2). On the contrary,

in a Luttinger liquid the spectral function, see Eq. (4), is manifestly non-Lorentzian. It diverges on the mass-shell $\epsilon = \xi_k$, vanishes at $\epsilon < \xi_k$, and decays slowly with ϵ at $\epsilon > \xi_k$.

We demonstrated that for a nonlinear dispersion relation with positive curvature, see Eq. (6), the domain where $A_k(\epsilon)$ differs from zero extends below the mass-shell, $\epsilon \geq \xi_k - k^2/m$. The mass-shell $\epsilon = \xi_k$ now falls within the domain of continuous spectrum. In this situation the Luttinger liquid result Eq. (4) is no longer valid. Instead of a one-sided power-law singularity at $\epsilon \rightarrow \xi_k$, [cf. Eq. (4)], the spectral function has a Lorentzian peak centered at the mass-shell. The width of the peak $1/\tau_k$, see Eq. (10), is much smaller than that in higher dimensions. In one dimension, the finite relaxation rate $1/\tau_k$ emerges only in the fourth order of the perturbation theory in the interaction strength and increases with k as k^8 (here k is momentum relative to p_F). At large enough momenta k , which are still exponentially small in the inverse interaction strength

$$k \gtrsim p_F e^{-a/\gamma_0^2}, \quad (128)$$

the Lorentzian peak in the spectral function carries most of the spectral weight. In other words, for k satisfying the inequality (128), the dispersion nonlinearity restores the Fermi liquid character of the particle part of the spectrum. The numerical coefficient a in the criterion (128) depends on the fraction of the spectral weight chosen to fall within the Lorentzian.

It should be emphasized that dispersion nonlinearity brings about particle-hole asymmetry into the problem. Indeed, we found that the nonlinearity does not affect qualitatively the hole region of the spectrum $\epsilon < 0$. The spectral function here resembles that in the Luttinger liquid, although with the modified value of the exponent.

Finally, we mention that the emergence of a finite quasiparticle lifetime brings some ramifications for the theory⁸ of the structure factor $S(q, \omega)$ of an interacting 1D fermion system. It smears the nonanalytical behavior of $S(q, \omega)$ at $\omega = vq + q^2/2m$. The smearing, however, affects only a tiny portion of the frequency interval $|\omega - vq| \lesssim q^2/2m$. Indeed, the width of the smearing region scales with q as $1/\tau_q \propto q^8/m^3$, while the width of the interval of interest is $q^2/2m$.

Acknowledgments

We thank Iddo Ussishkin for numerous discussions and for earlier collaboration which stimulated this work. This project was supported by DOE Grants DE-FG02-06ER46310 and DE-FG02-ER46311, and by A.P. Sloan foundation.

APPENDIX A: VERTEX CORRECTIONS

In this appendix we consider the dimensionless coupling vertex Γ characterizing the interaction of the d -particle with the bosonic field ϕ describing excitations within the subbands r and l , see Eq. (64). Our concern here is whether corrections to Γ due to interactions within the d -subband affect the leading logarithmic series considered in Section IV. The vertex depends on four variables, $\Gamma = \Gamma(\epsilon, k, \omega, q)$. The dependence of Γ on its arguments around the mass shell is not singular. It is clear then that the relevant object is the on-shell vertex correction

$$\delta\Gamma = \Gamma(\xi_k, k, \pm vq, q) - 1$$

(the bare value of the vertex is 1).

By construction of r, l -subbands (see Section IV A), the momentum q transferred to the bosonic field ϕ is restricted to $|q| \leq \lambda k$. Accordingly, the relevant frequencies $\omega = \pm vq$ satisfy $|\omega| \leq \lambda vk \ll \epsilon$. It then follows that the two d -particle Green functions adjacent to the bosonic field ϕ in the diagram such as that shown in Fig. 9(b) carry frequencies of the same sign, $\text{sgn}(\epsilon) = \text{sgn}(\epsilon + \omega)$. The on-shell vertex correction can then be expressed via the time-ordered d -particle self-energy $\Sigma_k^T(\epsilon)$ as

$$\delta\Gamma = \left. \frac{\partial \Sigma_k^T}{\partial \epsilon} \right|_{\epsilon \rightarrow \xi_k} + O(q). \quad (\text{A1})$$

The latter is discussed in details in Sections III and IV above. In the second order in $d-d$ interaction the self-energy is purely real and is given by $\Sigma^{(2)} \sim \gamma_0^2(\epsilon - \xi_k) \ln(\Lambda/\lambda)$, see Section IV. Eq. (A1) then yields

$$\text{Re } \delta\Gamma \sim \gamma_0^2 \ln(\Lambda/\lambda) \ll 1, \quad (\text{A2})$$

where we used Eq. (57). In the fourth order the self-energy acquires a finite imaginary part on the mass-shell, $\text{Im } \Sigma_k^{(4)}(\xi_k) = -1/2\tau_k$. Taking into account that $\text{Im } \Sigma_k^{(4)}$ varies with ϵ on the scale $\sim k^2/m$, and using Eq. (A1), we find

$$\text{Im } \delta\Gamma \sim \frac{1/\tau_k}{k^2/m} \ll 1. \quad (\text{A3})$$

According to Eqs. (A2) and (A3), vertex corrections due to interactions within d -subband are small. As far as the summation of the leading logarithmic contributions in Section IV is concerned, all such corrections can be safely neglected.

APPENDIX B: DERIVATION OF EQ. (72)

In this appendix we supply technical details needed to perform the Fourier transform of Eq. (71) leading to

Eq. (72). The coordinate integration can be performed at once. With the help of the convolution theorem, the remaining integral over time be written as

$$G_k \left(\epsilon; \frac{\Lambda k^2}{mv}, \Lambda k \right) = \int \frac{d\epsilon'}{2\pi} G_k^d(\epsilon - \epsilon') \mathcal{F}_k(\epsilon'), \quad (\text{B1})$$

where

$$G_k^d(\epsilon) = \frac{1}{\epsilon - \xi_k + i/2\tau_k} \quad (\text{B2})$$

is the bare d -particle Green function, see Eq. (59), and $\mathcal{F}_k(\epsilon)$ is given by

$$\begin{aligned} \mathcal{F}_k(\epsilon) &= \int dt e^{i\epsilon t} \left(1 + i \frac{\lambda k^2}{mv} (v_d + v)t \right)^{-\mu_+^2/4} \\ &\quad \times (1 - i \lambda k (v_d - v)t)^{-\mu_-^2/4}, \end{aligned} \quad (\text{B3})$$

where we denoted $\mu_- = \mu_k$ and $\mu_+ = \mu_{2p_F+k}$ for brevity. The integration in Eq. (B3) is carried out using the convolution theorem and the relation

$$\int \frac{dt e^{i\epsilon t}}{(1 \pm i\kappa t)^{\mu_{\pm}^2/4}} = \frac{2\pi}{\Gamma(\mu_{\pm}^2/4)} \frac{\theta(\pm\epsilon)}{|\epsilon|} \left| \frac{\epsilon}{\kappa} \right|^{\mu_{\pm}^2/4} e^{-|\epsilon|/\kappa}, \quad (\text{B4})$$

where $\kappa \sim \lambda k^2/m$. Taking into account that $v_d - v \approx k/m$ and $v_d + v \approx 2v$, we obtain for $\mu_{\pm} \ll 1$

$$\mathcal{F}_k(\epsilon) = \frac{\pi \mu_-^2 \mu_+^2}{8} \int d\epsilon' \frac{\theta(\epsilon') \theta(\epsilon' + \epsilon)}{\epsilon'(\epsilon' + \epsilon)} \left(\frac{\epsilon'}{\kappa} \right)^{\frac{\mu_-^2}{4}} \left(\frac{\epsilon' + \epsilon}{\kappa} \right)^{\frac{\mu_+^2}{4}}. \quad (\text{B5})$$

Eq. (B5) is valid for $|\epsilon| \lesssim \kappa = \lambda k^2/m$. In the case $\epsilon > 0$ we have

$$\mathcal{F}_k(\epsilon) = \frac{\pi \mu_+^2 \mu_-^2}{8\epsilon} \left(\frac{\epsilon}{\kappa} \right)^{\gamma_k^2} B(\mu_-^2/4, 1 - \gamma_k^2), \quad (\text{B6})$$

where $4\gamma_k^2 = \mu_-^2 + \mu_+^2$, see Eq. (8), and B is the standard beta-function. For weak interactions, $\mu_{\pm} \ll 1$, one finds $B \approx 4/\mu_-^2$. The case $\epsilon < 0$ is analyzed in a similar way. As a result, we obtain

$$\mathcal{F}_k(\epsilon) = \frac{\pi}{2\epsilon} \left| \frac{\epsilon}{\kappa} \right|^{\gamma_k^2} [\mu_+^2 \theta(\epsilon) + \mu_-^2 \theta(-\epsilon)], \quad (\text{B7})$$

covering both cases. We now substitute Eqs. (B2) and (B7) into Eq. (B1). Rewriting the integral in the latter equation as the contour integral we find

$$G_k \left(\epsilon; \frac{\Lambda k^2}{mv}, \Lambda k \right) = - (\lambda k^2/m)^{-\gamma_k^2} \left[\frac{\mu_{2p_F+k}^2}{4\gamma_k^2} \int_{C_+} \frac{dz}{2\pi i} \frac{(-z)^{\gamma_k^2-1}}{\epsilon - \xi_k + i/2\tau_k - z} - \frac{\mu_k^2}{4\gamma_k^2} \int_{C_-} \frac{dz}{2\pi i} \frac{z^{\gamma_k^2-1}}{\epsilon - \xi_k + i/2\tau_k - z} \right], \quad (\text{B8})$$

where the function z^α is chosen to have a cut in the complex plain along the negative real axis and contours C_\pm run clockwise around the positive (negative) half of the real axis. Closing the contours at infinity and taking the residue at $z = \epsilon - \xi_k + i/2\tau_k$ we arrive at Eq. (72).

APPENDIX C: DERIVATION OF EQ. (108)

Consider the operator

$$\Phi^\dagger(x) = \psi^{r\dagger}(-i\partial_x)\psi^{r\dagger} \quad (\text{C1})$$

entering Eq. (107). Proceeding in a standard fashion, we substitute here $\psi^r = \sqrt{k_0} e^{i\varphi}$ with $\varphi \equiv \varphi^r$, see Eq. (86), and write the derivative as a finite difference,

$$\Phi^\dagger(x) = \frac{-ik_0}{2\Delta} e^{-i\varphi(x)} \left[e^{-i\varphi(x+\Delta)} - e^{-i\varphi(x-\Delta)} \right]. \quad (\text{C2})$$

On making use of the identity

$$e^a e^b = : e^{a+b} : e^{\langle ab + \frac{1}{2}(a^2+b^2) \rangle}$$

valid for any operators a and b which are *linear* in bosonic fields (the colons denote the normal ordering), we find

$$e^{-i\varphi(x)} e^{-i\varphi(x\pm\Delta)} = e^{-2\langle\varphi^2(0)\rangle} : e^{-i[\varphi(x)+\varphi(x\pm\Delta)]} : \times (1 \pm 2\pi i k_0 \Delta).$$

We now approximate here

$$: e^{-i[\varphi(x)+\varphi(x\pm\Delta)]} : \approx : e^{-2i\varphi(x)} : = e^{2\langle\varphi^2(0)\rangle - 2i\varphi(x)},$$

so that

$$e^{-i\varphi(x)} e^{-i\varphi(x\pm\Delta)} \approx e^{-2i\varphi(x)} (1 \pm 2\pi i k_0 \Delta). \quad (\text{C3})$$

Eqs. (C2) and (C3) yield

$$\Phi^\dagger(x) = 2\pi k_0^2 e^{-2i\varphi(x)}. \quad (\text{C4})$$

Substituting this expression into $\Psi^\dagger = \Phi^\dagger \psi^d$ [see Eqs. (107) and (C1)], we arrive at Eq. (108).

-
- ¹ A.M. Chang, Rev. Mod. Phys. **75**, 1449 (2003).
² J.W.G. Wilder, L.C. Venema, A.G. Rinzler, R.E. Smalley, and C. Dekker, Nature **391**, 59 (1998); M. Bockrath, D.H. Cobden, A.G. Rinzler, R.E. Smalley, L. Balents, and P.L. McEuen, Nature **397**, 568 (1999).
³ O.M. Auslaender, H. Steinberg, A. Yacoby, Y. Tserkovnyak, B.I. Halperin, R. de Picciotto, K.W. Baldwin, L.N. Pfeiffer, K.W. West, Sol. State Commun. **131**, 657 (2004).
⁴ B. Lake, D.A. Tennant, C.D. Frost, and S.E. Nagler, Nature Materials **4**, 329 (2005).
⁵ A. Görlitz, J.M. Vogels, A.E. Leanhardt, C. Raman, T.L. Gustavson, J.R. Abo-Shaeer, A.P. Chikkatur, S. Gupta, S. Inouye, T. Rosenband, and W. Ketterle, Phys. Rev. Lett. **87**, 130402 (2001); M. Greiner, I. Bloch, O. Mandel, T.W. Hänsch, T. Esslinger, Appl. Phys. B **73**, 769, (2004).
⁶ M. Pustilnik, E.G. Mishchenko, L.I. Glazman, and A.V. Andreev, Phys. Rev. Lett. **91**, 126805 (2003).
⁷ A.G. Abanov and P. Wiegmann, Phys. Rev. Lett. **95**, 076402 (2005).
⁸ M. Pustilnik, M. Khodas, A. Kamenev, and L.I. Glazman, Phys. Rev. Lett. **96**, 196405 (2006).
⁹ R.G. Pereira, J. Sirker, J.-S. Caux, R. Hagemans, J. M. Maillet, S. R. White, and I. Affleck, Phys. Rev. Lett. **96**, 257202 (2006).
¹⁰ M. Pustilnik, Phys. Rev. Lett. **97**, 036404 (2006).
¹¹ S. Teber, Eur. Phys. Journ. B **52**, 233 (2006).
¹² J.-S. Caux and J.M. Maillet, Phys. Rev. Lett. **95**, 077201 (2005), J.-S. Caux, R. Hagemans, and J.M. Maillet, J. Stat. Mech. P09003 (2005).
¹³ S. Tomonaga, Prog. Theor. Phys. **5**, 544 (1950).
¹⁴ J.M. Luttinger, J. Math. Phys. **4**, 1154 (1963).
¹⁵ D.C. Mattis and E.H. Lieb, J. Math. Phys. **6**, 375 (1965).
¹⁶ P. Nozières, *Theory of Interacting Fermi Systems* (Addison-Wesley, 1997).
¹⁷ I.E. Dzyaloshinskii and A.I. Larkin, Zh. Eksp. Teor. Fiz. **65**, 411 (1973) [Sov. Phys. JETP **38**, 202 (1974)].
¹⁸ A. Luther and I. Peschel, Phys. Rev. B **9**, 2911 (1974).
¹⁹ Spectral function for TL model at $T > 0$ is considered in details in K. Le Hur, Phys. Rev. B **74**, 165104 (2006).
²⁰ F.D.M. Haldane, J. Phys. C **14**, 2585 (1981).
²¹ We assume that the interaction potential is sufficiently smooth so that $V_{2k_F} \ll V_0$. We also stay away from *integrable* models. In such models, multi-particle collisions such as those discussed in Section IIC are absent²⁸, and $1/\tau_k$ vanishes identically. This can be seen already in perturbation theory, as discussed in Section VI for $V_q \propto |q|$ (Calogero-Sutherland model) and in Ref. [25] for $V_q \propto q^2$.
²² P. W. Anderson, Phys. Rev. Lett. **18**, 1049 (1967).
²³ G.D. Mahan, *Many-Particle Physics* (Springer, 2000).
²⁴ F.D.M. Haldane Phys. Rev. Lett. **47**, 1840 (1981).
²⁵ A.M. Lunde, K. Flensberg, and L.I. Glazman, Phys. Rev. B **75**, 245418 (2007).
²⁶ I. Ussishkin and L.I. Glazman, unpublished.

- ²⁷ J. Solyom, *Adv. Phys.*, **28**, 201 (1979).
- ²⁸ B. Sutherland, *Beautiful Models* (World Scientific, 2004).
- ²⁹ M.R. Zirnbauer and F.D.M. Haldane, *Phys. Rev. B* **52**, 8729 (1995); D. Serban, F. Lesage, and V. Pasquier, *Nucl. Phys. B* **466**, 499 (1996).
- ³⁰ F.D.M. Haldane, in *Proceedings of the 16th Taniguchi Symposium*, eds. A. Okiji and N. Kawakami (Springer, Berlin, 1994); P.J. Forrester, *J. Math. Phys.* **36**, 86 (1995); Z.N.C. Ha, *Phys. Rev. Lett.* **73**, 1574 (1994); Z.N.C. Ha, *Nucl. Phys. B* **435**, 604 (1995); F. Lesage, V. Pasquier, and D. Serban, *Nucl. Phys. B* **435**, 585 (1995).
- ³¹ A.P. Polychronakos, *J. Phys. A* **39**, 12793 (2006).